The Astrophysical Journal Supplement Series, 247:70 (11pp), 2020 April https://doi.org/10.3847/1538-4365/ab7cc6

Large-scale Multiconfiguration Dirac–Hartree–Fock Calculations for Astrophysics: $n = 4$ Levels in P-like Ions from Mn XI to Ni XIV

C. X. Song[1], K. Wang[1,2], G. Del Zanna[3], P. Jönsson[4], R. Si[5], M. Godefroid[5], G. Gaigalas[6], L. Radžiūtė[6], P. Rynkun[6], X. H. Zhao[1], J. Yan[7], and C. Y. Chen[2]

[1] Hebei Key Lab of Optic-electronic Information and Materials, The College of Physics Science and Technology, Hebei University, Baoding 071002, People's Republic of China; wang_kai10@fudan.edu.cn
[2] Shanghai EBIT Lab, Key Laboratory of Nuclear Physics and Ion-beam Application, Institute of Modern Physics, Department of Nuclear Science and Technology, Fudan University, Shanghai 200433, People's Republic of China
[3] DAMTP, Centre for Mathematical Sciences, University of Cambridge, Wilberforce Road, Cambridge CB3 0WA, UK
[4] Group for Materials Science and Applied Mathematics, Malmö University, SE-20506, Malmö, Sweden
[5] Spectroscopy, Quantum Chemistry and Atmospheric Remote Sensing, CP160/09, Université libre de Bruxelles, B-1050 Brussels, Belgium
[6] Institute of Theoretical Physics and Astronomy, Vilnius University, Saulėtekio av. 3, LT-10222, Vilnius, Lithuania
[7] Institute of Applied Physics and Computational Mathematics, Beijing 100088, People's Republic of China
Received 2020 January 18; accepted 2020 February 28; published 2020 April 14

Abstract

Using the multiconfiguration Dirac–Hartree–Fock and the relativistic configuration interaction methods, a consistent set of transition energies and radiative transition data for the lowest 546 (623, 701, and 745) states of the $3p^4 3d$, $3s3p^2 3d^2$, $3s3p^3 4p$, $3s3p^4$, $3s^2 3d^3$, $3s^2 3p^2 3d$, $3s^2 3p^2 4d$, $3s^2 3p^2 4s$, $3p^3 3d^2$, $3p^5$, $3s3p3d^3$, $3s3p^3 3d$, $3s3p^3 4s$, $3s^2 3p3d^2$, $3s^2 3p^2 4p$, and $3s^2 3p^3$ configurations in Mn XI (Fe XII, Co XIII, and Ni XIV) is provided. The comparison between calculated excitation energies for the $n = 4$ states and available experimental values for Fe XII indicate that the calculations are highly accurate, with uncertainties of only a few hundred cm^{-1}. Lines from these states are prominent in the soft X-rays. With the present calculations, several recent new identifications are confirmed. Other identifications involving $3p^2 4d$ levels in Fe XII that were found to be questionable are discussed and a few new assignments are recommended. As some $n = 4$ states of the other ions also show large discrepancies between experimental and calculated energies, we reassess their identification. The present study provides highly accurate atomic data for the $n = 4$ states of P-like ions of astrophysical interest, for which experimental data are scarce.

Unified Astronomy Thesaurus concepts: Atomic data benchmarking (2064); Laboratory astrophysics (2004)

Supporting material: machine-readable tables

1. Introduction

In the ultraviolet (UV) and extreme ultraviolet (EUV) spectral regions, P-like ions of the iron group elements are used for plasma diagnostics, especially to measure electron densities (see, e.g., the review by Del Zanna & Mason 2018). Fe XII is especially important for the solar corona. The most prominent lines in the UV/EUV region were observed by Solar and Heliospheric Observatory and Skylab and were recently measured by the Hinode satellite (Young et al. 2009; Del Zanna 2012a). In our recent work (Wang et al. 2018b), using the multiconfiguration Dirac–Hartree–Fock (MCDHF) and the relativistic configuration interaction (RCI) methods (Grant 2007; Froese Fischer et al. 2016), excitation energies for the lowest 143 states of the $n = 3$ ($3s^2 3p^3$, $3s3p^4$, $3s^2 3p^2 3d$, $3s3p^3 3d$, $3p^5$, and $3s^2 3p3d^2$) configurations from Cr X to Zn XVI were provided. Using these data, we reassessed the previous identifications of the important $3s^2 3p^2 3d$ levels in Fe XII, confirming most of the previous suggestions by Del Zanna & Mason (2005). Based on our calculated energies, the atomic data from Del Zanna et al. (2012a), and Hinode EUV imaging spectrometer spectra, new identifications of a few $3s3p^3 3d$ levels were also suggested, which have been included in the CHIANTI atomic database version 9 (Dere et al. 1997, 2019).

The $n = 4 \rightarrow n = 3$ transitions in highly ionized Fe ions, including Fe XII, are the dominant lines in the soft X-rays (50–150 Å). These transitions have recently been reviewed by Del Zanna (2012b), where a series of large-scale scattering calculations (the first of its kind) for all the ions, provided by Del Zanna (2012b) and Del Zanna et al. (2012a, 2012b) in a series of papers, were used to assess the identifications in this spectral region. Most of the previous identifications of these $n = 4 \rightarrow n = 3$ transitions were due to Fawcett et al. (1972), although some of the original ones were due to Edlén in his seminal work in the 1930s (see, e.g., the review in Del Zanna & Mason 2018). Del Zanna (2012b) pointed out that several of the strongest transitions were never assigned and proposed their identification, based on solar and laboratory spectra (the same used by Fawcett et al. 1972). A few problems with Fawcett's assignments were also noted, but the accuracy of the theoretical wavelengths did not allow firm identifications.

A significant fraction (about a third) of the spectral lines in the soft X-rays still awaits interpretation. One purpose of our work is to provide excitation energies and wavelengths involving the $n = 4$ states for P-like ions from Mn XI to Ni XIV with spectroscopic accuracy, to aid the identification process. Using the MCDHF and RCI method (in the following, referred to as MCDHF), excitation energies, wavelengths, lifetimes, and radiative transition data including oscillator strengths, line strengths, and transition rates, are provided for the main $n = 3$, 4 levels of the $3p^4 3d$, $3s3p^2 3d^2$, $3s3p^3 4p$, $3s3p^4$, $3s^2 3d^3$, $3s^2 3p^2 3d$, $3s^2 3p^2 4d$, $3s^2 3p^2 4s$, $3p^3 3d^2$, $3p^5$, $3s3p3d^3$, $3s3p^3 3d$, $3s3p^3 4s$, $3s^2 3p3d^2$, $3s^2 3p^2 4p$, and $3s^2 3p^3$ configurations. In Section 3, using accurate wavelengths for the $n = 4 \rightarrow n = 3$ transitions of Fe XII to Ni XIV, we will review

Table 1
Excitation Energies E in cm^{-1} for 623 States of Fe XII from the Present MCDHF1 Calculations

Key	Level	E_{MCDHF1}	E_{MCDHF2}	ΔE_{MCDHF2}	E_{NIST}	ΔE_{NIST}	$E_{CHIANTI1}$	$\Delta E_{CHIANTI1}$	$E_{CHIANTI2}$	$\Delta E_{CHIANTI2}$
1	$3s^2\ 3p^3(^4_3S)\ ^4S^o_{3/2}$	0	0	0	0	0	0		0	0
2	$3s^2\ 3p^3(^2_3D)\ ^2D^o_{3/2}$	41872	41771	−101	41566	−306	41555.602	−316.398	41556	−316
3	$3s^2\ 3p^3(^2_3D)\ ^2D^o_{5/2}$	46386	46320	−66	46075	−311	46088	−298	46088	−298
4	$3s^2\ 3p^3(^2_1P)\ ^2P^o_{1/2}$	74557	74373	−185	74109	−448	74107	−450	74107	−450
5	$3s^2\ 3p^3(^2_1P)\ ^2P^o_{3/2}$	80926	80763	−163	80515	−411	80515	−411	80515	−411
6	$3s\ ^2S\ 3p^4(^3_2P)\ ^4P_{5/2}$	274618	274499	−119	274373	−245	274373	−245	274373	−245
7	$3s\ ^2S\ 3p^4(^3_2P)\ ^4P_{3/2}$	284240	284127	−114	284005	−235	284005	−235	277374	−6866
8	$3s\ ^2S\ 3p^4(^3_2P)\ ^4P_{1/2}$	288550	288452	−98	288307	−243	288307	−243	288307	−243
9	$3s\ ^2S\ 3p^4(^1_2D)\ ^2D_{3/2}$	340143	340105	−38	340020	−123	339725	−418	335258	−4885
10	$3s\ ^2S\ 3p^4(^1_2D)\ ^2D_{5/2}$	342090	342051	−39	341703	−387	341716	−374	341716	−374

Note. For comparison, excitation energies from our recent MCDHF2 calculations (MCDHF2; Wang et al. 2018b), experimental excitation energies compiled in the NIST ASD (Kramida et al. 2018), experimental (CHIANTI1) and calculated (CHIANTI2) values from the CHIANTI version 9 (Dere et al. 1997, 2019) are also included, along with their differences ($\Delta E_x = E_x - E_{MCDHF1}$) in cm^{-1} with the present MCDHF values.

(This table is available in its entirety in machine-readable form.)

their identification and suggest some new lines. This provides a stringent accuracy assessment of our calculations.

The other purpose of our work is to provide a consistent accurate set of radiative transition data for P-like ions from Mn XI to Ni XIV for spectral line modeling. This work extends and complements our long-term theoretical efforts (Wang et al. 2014, 2015, 2016a, 2016b, 2017a, 2017b, 2017c, 2017d, 2018a, 2018b, 2018c, 2018d, 2019, 2020; Guo et al. 2015, 2016; Si et al. 2016, 2017, 2018; Chen et al. 2017, 2018; Zhao et al. 2018) to provide atomic data for L- and M-shell systems with high accuracy. For a review, see Jönsson et al. (2017).

2. Theory and Calculations

The MCDHF method in the GRASP2K code (Jönsson et al. 2007, 2013) is reviewed by Froese Fischer et al. (2016). This method is also described in our recent papers (Wang et al. 2018b, 2018c). For this reason, in the sections below, only the computational procedures are described.

In our MCDHF calculations, the multireference (MR) sets for even and odd parities include even configurations: $3p^43d$, $3s3p^23d^2$, $3s3p^34p$, $3s3p^4$, $3s^23d^3$, $3s^23p^23d$, $3s^23p^24d$, and $3s^23p^24s$; odd configurations: $3p^33d^2$, $3p^5$, $3s3p3d^3$, $3s3p^33d$, $3s3p^34s$, $3s^23p3d^2$, $3s^23p^24f$, $3s^23p^24p$, and $3s^23p^3$.

By allowing single and double substitutions from the $n = 3$, 4 electrons of the MR sets to orbitals with $n \leqslant 8$, $l \leqslant 6$, and by allowing single excitations of the $n = 2$ electrons to orbitals with $n \leqslant 6$, $l \leqslant 4$, configuration state function (CSF) expansions are generated. The $1s$ shell is defined as inactive closed shell in all CSFs of the expansions.

For both energy separations and transition probabilities, the neglected correlations from $n = 1$, 2 are comparatively unimportant (Wang et al. 2018b). In the following RCI calculation, the transverse electron interaction in the low-frequency limit and the leading quantum electrodynamic (QED) effects (vacuum polarization and self-energy) corrections are included. In the final CSF expansions for the different J symmetries, the number of CSFs is, respectively, about 5.9 millions for even parity and 8.1 millions for odd parity.

By using the *jj-LSJ* transformation approach (Gaigalas et al. 2004, 2017), the *jj*-coupled CSFs are transformed into *LSJ*-coupled CSFs, from which the *LSJ* labels used by experimentalists are obtained.

3. Evaluation of Data

3.1. Energy Levels

In Table 1, excitation energies for the lowest 623 levels of the $3p^43d$, $3s3p^23d^2$, $3s3p^34p$, $3s3p^4$, $3s^23d^3$, $3s^23p^23d$, $3s^23p^24d$, $3s^23p^24s$, $3p^33d^2$, $3p^5$, $3s3p3d^3$, $3s3p^33d$, $3s3p^34s$, $3s^23p3d^2$, $3s^23p^24p$, and $3s^23p^3$ configurations in Fe XII from the present MCDHF calculations (hereafter referred to as MCDHF1) are displayed. All these states are below the first $3s^23p^24f$ level. For comparison, experimental excitation energies compiled in the Atomic Spectra Database (ASD) of the National Institute of Standards and Technology (NIST; Kramida et al. 2018), while experimental (CHIANTI1) and calculated (CHIANTI2) values from the CHIANTI version 9 (Dere et al. 1997, 2019) are also included along with excitation energies from our recent MCDHF calculations (MCDHF2; Wang et al. 2018b). The previous calculations, such as Tayal (2011), Storey et al. (2005), and Vilkas & Ishikawa (2004), were focused on the $n = 3$ levels, and their comparison with our recently MCDHF results for the $n = 3$ levels was shown in our previous work (Wang et al. 2018b). Therefore, their results (Vilkas & Ishikawa 2004; Storey et al. 2005; Tayal 2011) are not included in Table 1.

The differences between the MCDHF1 and MCDHF2 results for the lowest 143 states are listed in Table 1 and are generally within a few hundred cm^{-1}. The average absolute difference with the standard deviation (Wang et al. 2017c) between the two data sets is $1\,cm^{-1} \pm 313\,cm^{-1}$. When the present MCDHF1 excitation energies for the $n = 3$ levels are compared with the experimental values from the NIST and CHIANTI database, the agreement is also very good. The differences are generally within a few hundred cm^{-1}. There is a misprint for experimental excitation energies of the two levels $(3s^2\ 3p^2(^1_2D)\ ^1D\ 3d\ ^2P_{3/2}$ with the key (#37) and $\#38/3s^2\ 3p^2(^1_2D)\ ^1D\ 3d\ ^2S_{1/2})$ in the CHIANTI version 9. The experimental values should be 577,680 cm^{-1} for the $\#37/3s^2\ 3p^2(^1_2D)\ ^1D\ 3d\ ^2P_{3/2}$ level and 579,630 cm^{-1} for the $\#38/3s^2\ 3p^2(^1_2D)\ ^1D\ 3d\ ^2S_{1/2}$ level, respectively (Del Zanna & Mason 2005). After correcting this

Table 2
Excitation Energies in cm^{-1} for the 546 (623, 701, and 745) Lowest Levels of Mn XI (Fe XII, Co XIII, and Ni XIV), as well as Radiative Lifetimes (in s)

Z	Key	Level	$J\pi$	E_{MCDHF}	E_{NIST}	ΔE	τ^{l}_{MCDHF}	τ^{v}_{MCDHF}	*LS*-composition
25	1	$3s^2\ 3p^3(^4_3S)\ ^4S^o_{3/2}$	3/2−	0	0	0			$0.95 + 0.02\ 3s\ ^2S\ 3p^3(^2_3D)\ ^3D\ 3d\ ^4S^o$
25	2	$3s^2\ 3p^3(^2_3D)\ ^2D^o_{3/2}$	3/2−	39688	39384	304	3.65E−02	3.65E−02	$0.87 + 0.09\ 3s^2\ 3p^3(^2_1P)\ ^2P^o$
25	3	$3s^2\ 3p^3(^2_3D)\ ^2D^o_{5/2}$	5/2−	42986	42702	284	7.49E−01	7.49E−01	0.96
25	4	$3s^2\ 3p^3(^2_1P)\ ^2P^o_{1/2}$	1/2−	69389	68945	444	6.34E−03	6.34E−03	0.95
25	5	$3s^2\ 3p^3(^2_1P)\ ^2P^o_{3/2}$	3/2−	73967	73552	415	2.63E−03	2.63E−03	$0.84 + 0.10\ 3s^2\ 3p^3(^2_3D)\ ^2D^o$
25	6	$3s\ ^2S\ 3p^4(^3_2P)\ ^4P_{5/2}$	5/2+	254257	253974	283	7.05E−10	6.83E−10	$0.88 + 0.09\ 3s^2\ 3p^2(^3_2P)\ ^3P\ 3d\ ^4P$
25	7	$3s\ ^2S\ 3p^4(^3_2P)\ ^4P_{3/2}$	3/2+	261964	261683	281	6.60E−10	6.43E−10	$0.88 + 0.10\ 3s^2\ 3p^2(^3_2P)\ ^3P\ 3d\ ^4P$
25	8	$3s\ ^2S\ 3p^4(^3_2P)\ ^4P_{1/2}$	1/2+	265557	265144	413	6.30E−10	6.16E−10	$0.87 + 0.10\ 3s^2\ 3p^2(^3_2P)\ ^3P\ 3d\ ^4P$
25	9	$3s\ ^2S\ 3p^4(^1_2D)\ ^2D_{3/2}$	3/2+	314904	314532	372	3.19E−10	3.10E−10	$0.76 + 0.17\ 3s^2\ 3p^2(^1_2D)\ ^1D\ 3d\ ^2D + 0.03\ 3s^2\ 3p^2(^1_0S)\ ^1S\ 3d\ ^2D$
25	10	$3s\ ^2S\ 3p^4(^1_2D)\ ^2D_{5/2}$	5/2+	316295	315881	414	3.48E−10	3.37E−10	$0.76 + 0.17\ 3s^2\ 3p^2(^1_2D)\ ^1D\ 3d\ ^2D + 0.03\ 3s^2\ 3p^2(^1_0S)\ ^1S\ 3d\ ^2D$
25	11	$3s\ ^2S\ 3p^4(^3_2P)\ ^2P_{3/2}$	3/2+	361638	361400	238	1.22E−10	1.19E−10	$0.46 + 0.45\ 3s^2\ 3p^2(^3_2P)\ ^3P\ 3d\ ^2P + 0.05\ 3s^2\ 3p^2(^1_2D)\ ^1D\ 3d\ ^2P$
25	12	$3s^2\ 3p^2(^3_2P)\ ^3P\ 3d\ ^2P_{1/2}$	1/2+	366070	*365689*	381	1.11E−10	1.09E−10	$0.31 + 0.35\ 3s\ ^2S\ 3p^4(^3_2P)\ ^2P + 0.23\ 3s\ ^2S\ 3p^4(^1_0S)\ ^2S$
25	13	$3s\ ^2S\ 3p^4(^1_0S)\ ^2S_{1/2}$	1/2+	379642	379093	549	1.34E−10	1.31E−10	$0.57 + 0.14\ 3s^2\ 3p^2(^3_2P)\ ^3P\ 3d\ ^2P + 0.12\ 3s\ ^2S\ 3p^4(^3_2P)\ ^2P$
25	26	$3s^2\ 3p^2(^3_2P)\ ^3P\ 3d\ ^2P_{3/2}$	3/2+	467541	467240	301	1.66E−11	1.64E−11	$0.24 + 0.42\ 3s\ ^2S\ 3p^4(^3_2P)\ ^2P + 0.26\ 3s^2\ 3p^2(^1_2D)\ ^1D\ 3d\ ^2P$
25	27	$3s^2\ 3p^2(^3_2P)\ ^3P\ 3d\ ^4P_{5/2}$	5/2+	477149	477170	−21	1.28E−11	1.27E−11	$0.83 + 0.09\ 3s\ ^2S\ 3p^4(^3_2P)\ ^4P$
25	28	$3s\ ^2S\ 3p^4(^3_2P)\ ^2P_{1/2}$	1/2+	477269	*476980*	289	1.65E−11	1.63E−11	$0.39 + 0.30\ 3s^2\ 3p^2(^1_2D)\ ^1D\ 3d\ ^2P + 0.21\ 3s^2\ 3p^2(^3_2P)\ ^3P\ 3d\ ^2P$
25	29	$3s^2\ 3p^2(^3_2P)\ ^3P\ 3d\ ^4P_{3/2}$	3/2+	480737	480720	17	1.26E−11	1.25E−11	$0.82 + 0.09\ 3s\ ^2S\ 3p^4(^3_2P)\ ^4P + 0.02\ 3s^2\ 3p^2(^1_0S)\ ^1S\ 3d\ ^2D$
25	30	$3s^2\ 3p^2(^3_2P)\ ^3P\ 3d\ ^4P_{1/2}$	1/2+	483070	483040	30	1.21E−11	1.21E−11	$0.82 + 0.09\ 3s\ ^2S\ 3p^4(^3_2P)\ ^4P + 0.02\ 3s\ ^2S\ 3p^4(^3_2P)\ ^2P$
25	33	$3s^2\ 3p^2(^1_2D)\ ^1D\ 3d\ ^2D_{3/2}$	3/2+	515486	515210	276	1.53E−11	1.52E−11	$0.76 + 0.14\ 3s\ ^2S\ 3p^4(^1_2D)\ ^2D + 0.03\ 3s^2\ 3p^2(^1_0S)\ ^1S\ 3d\ ^2D$
25	34	$3s^2\ 3p^2(^1_2D)\ ^1D\ 3d\ ^2D_{5/2}$	5/2+	515724	515430	294	2.15E−11	2.13E−11	$0.68 + 0.17\ 3s^2\ 3p^2(^1_0S)\ ^1S\ 3d\ ^2D + 0.10\ 3s\ ^2S\ 3p^4(^1_2D)\ ^2D$
25	35	$3s^2\ 3p^2(^1_2D)\ ^1D\ 3d\ ^2P_{1/2}$	1/2+	530912	530620	292	1.59E−11	1.58E−11	$0.56 + 0.23\ 3s^2\ 3p^2(^3_2P)\ ^3P\ 3d\ ^2P + 0.09\ 3s^2\ 3p^2(^1_2D)\ ^1D\ 3d\ ^2S$
25	36	$3s^2\ 3p^2(^1_2D)\ ^1D\ 3d\ ^2P_{3/2}$	3/2+	537094	536800	294	1.55E−11	1.54E−11	$0.61 + 0.27\ 3s^2\ 3p^2(^3_2P)\ ^3P\ 3d\ ^2P + 0.06\ 3s\ ^2S\ 3p^4(^3_2P)\ ^2P$
25	39	$3s^2\ 3p^2(^3_2P)\ ^3P\ 3d\ ^2F_{7/2}$	7/2+	541095	541030	65	1.03E−11	1.03E−11	$0.59 + 0.36\ 3s^2\ 3p^2(^1_2D)\ ^1D\ 3d\ ^2F$
25	40	$3s^2\ 3p^2(^3_2P)\ ^3P\ 3d\ ^2D_{5/2}$	5/2+	561720	561400	320	1.15E−11	1.15E−11	$0.51 + 0.26\ 3s^2\ 3p^2(^1_0S)\ ^1S\ 3d\ ^2D + 0.07\ 3s^2\ 3p^2(^3_2P)\ ^3P\ 3d\ ^2F$
25	41	$3s^2\ 3p^2(^3_2P)\ ^3P\ 3d\ ^2D_{3/2}$	3/2+	563354	563060	294	1.18E−11	1.17E−11	$0.56 + 0.36\ 3s^2\ 3p^2(^1_0S)\ ^1S\ 3d\ ^2D$
25	227	$3s^2\ 3p^2(^3_2P)\ ^3P\ 4s\ ^4P_{1/2}$	1/2+	1078017	1078200	−183	1.52E−11	1.52E−11	$0.87 + 0.03\ 3s^2\ 3p^2(^3_2P)\ ^3P\ 4s\ ^2P + 0.02\ 3s^2\ 3p^2(^1_0S)\ ^1S\ 4s\ ^2S$
25	231	$3s^2\ 3p^2(^3_2P)\ ^3P\ 4s\ ^4P_{3/2}$	3/2+	1084219	1084130	89	1.60E−11	1.60E−11	$0.91 + 0.02\ 3s^2\ 3p^2(^3_2P)\ ^3P\ 4s\ ^2P$
25	236	$3s^2\ 3p^2(^3_2P)\ ^3P\ 4s\ ^4P_{5/2}$	5/2+	1091274	1091160	114	1.62E−11	1.62E−11	$0.88 + 0.05\ 3s^2\ 3p^2(^1_2D)\ ^1D\ 4s\ ^2D$
25	244	$3s^2\ 3p^2(^3_2P)\ ^3P\ 4s\ ^2P_{3/2}$	3/2+	1103073	1102840	233	5.80E−12	5.81E−12	$0.79 + 0.12\ 3s^2\ 3p^2(^1_2D)\ ^1D\ 4s\ ^2D$
25	252	$3s^2\ 3p^2(^1_2D)\ ^1D\ 4s\ ^2D_{5/2}$	5/2+	1121369	1120870	499	1.06E−11	1.06E−11	$0.69 + 0.05\ 3s\ ^2S\ 3p^2(^1_2D)\ ^2D\ 3d^2(^1_2D)\ ^2D + 0.05\ 3p^4(^3_2P)\ ^3P\ 3d\ ^2D$
25	255	$3s^2\ 3p^2(^1_2D)\ ^1D\ 4s\ ^2D_{3/2}$	3/2+	1122276	1121880	396	9.98E−12	9.98E−12	$0.58 + 0.08\ 3s^2\ 3p^2(^3_2P)\ ^3P\ 4s\ ^2P + 0.05\ 3p^4(^3_2P)\ ^3P\ 3d\ ^2D$
25	422	$3s^2\ 3p^2(^3_2P)\ ^3P\ 4d\ ^4P_{5/2}$	5/2+	1325082	1324910	172	7.75E−12	7.68E−12	$0.46 + 0.23\ 3s^2\ 3p^2(^3_2P)\ ^3P\ 4d\ ^4F + 0.11\ 3s^2\ 3p^2(^3_2P)\ ^3P\ 4d\ ^4D$
25	432	$3s^2\ 3p^2(^3_2P)\ ^3P\ 4d\ ^4F_{5/2}$	5/2+	1329453	1329310	143	1.11E−11	1.10E−11	$0.54 + 0.35\ 3s^2\ 3p^2(^3_2P)\ ^3P\ 4d\ ^4P + 0.04\ 3s^2\ 3p^2(^3_2P)\ ^3P\ 4d\ ^2F$
25	433	$3s^2\ 3p^2(^3_2P)\ ^3P\ 4d\ ^4P_{3/2}$	3/2+	1331432	1332280	−848	6.44E−12	6.38E−12	$0.50 + 0.16\ 3s\ ^2S\ 3p^2(^3_2P)\ ^2P\ 3d^2(^1_0S)\ ^2P + 0.10\ 3s\ ^2S\ 3p^2(^1_0S)\ ^2S\ 3d^2(^3_2P)\ ^2P$
25	437	$3s^2\ 3p^2(^3_2P)\ ^3P\ 4d\ ^2F_{5/2}$	5/2+	1333831	1331340	**2491**	9.86E−12	9.76E−12	$0.73 + 0.11\ 3s^2\ 3p^2(^3_2P)\ ^3P\ 4d\ ^4F + 0.05\ 3s^2\ 3p^2(^1_2D)\ ^1D\ 4d\ ^2F$
25	440	$3s^2\ 3p^2(^3_2P)\ ^3P\ 4d\ ^2F_{7/2}$	7/2+	1340574	1336860	**3714**	1.53E−11	1.51E−11	$0.57 + 0.17\ 3s^2\ 3p^2(^3_2P)\ ^3P\ 4d\ ^4D + 0.09\ 3s^2\ 3p^2(^3_2P)\ ^3P\ 4d\ ^4F$
25	455	$3s^2\ 3p^2(^3_2P)\ ^3P\ 4d\ ^4D_{7/2}$	7/2+	1345585	1345410	175	8.68E−12	8.59E−12	$0.56 + 0.26\ 3s^2\ 3p^2(^3_2P)\ ^3P\ 4d\ ^2F + 0.09\ 3s^2\ 3p^2(^1_2D)\ ^1D\ 4d\ ^2F$
25	462	$3s^2\ 3p^2(^3_2P)\ ^3P\ 4d\ ^2D_{5/2}$	5/2+	1348983	1348630	353	6.22E−12	6.15E−12	$0.65 + 0.22\ 3s^2\ 3p^2(^1_2D)\ ^1D\ 4d\ ^2F + 0.05\ 3s^2\ 3p^2(^1_2D)\ ^1D\ 4d\ ^2D$
25	464	$3s^2\ 3p^2(^3_2P)\ ^3P\ 4d\ ^2D_{3/2}$	3/2+	1350549	1350080	469	6.15E−12	6.05E−12	$0.83 + 0.03\ 3s^2\ 3p^2(^3_2P)\ ^3P\ 4d\ ^2P + 0.03\ 3s^2\ 3p^2(^1_2D)\ ^1D\ 4d\ ^2D$
25	478	$3s^2\ 3p^2(^1_2D)\ ^1D\ 4d\ ^2F_{7/2}$	7/2+	1360953	1360590	363	8.94E−12	8.86E−12	$0.77 + 0.13\ 3s^2\ 3p^2(^3_2P)\ ^3P\ 4d\ ^4D + 0.02\ 3s^2\ 3p^2(^3_2P)\ ^3P\ 4d\ ^4F$
25	481	$3s^2\ 3p^2(^1_2D)\ ^1D\ 4d\ ^2F_{5/2}$	5/2+	1362080	1361630	450	6.22E−12	6.16E−12	$0.47 + 0.18\ 3s^2\ 3p^2(^1_2D)\ ^1D\ 4d\ ^2D + 0.08\ 3s^2\ 3p^2(^3_2P)\ ^3P\ 4d\ ^2D$
25	489	$3s^2\ 3p^2(^1_2D)\ ^1D\ 4d\ ^2D_{5/2}$	5/2+	1365951	1362940	**3011**	4.67E−12	4.61E−12	$0.50 + 0.16\ 3s^2\ 3p^2(^3_2P)\ ^3P\ 4d\ ^2D + 0.14\ 3s^2\ 3p^2(^1_2D)\ ^1D\ 4d\ ^2F$

Table 2
(Continued)

Z	Key	Level	$J\pi$	$E_{\rm MCDHF}$	$E_{\rm NIST}$	ΔE	$\tau^{l}_{\rm MCDHF}$	$\tau^{v}_{\rm MCDHF}$	LS-composition
25	511	$3s^2\ 3p^2(^1_2D)\ ^1D\ 4d\ \ ^2S_{1/2}$	1/2+	1384507	1374650	**9857**	9.66E−12	9.53E−12	0.9
26	1	$3s^2\ 3p^3(^4_3S)\ \ ^4S^{\circ}_{3/2}$	3/2−	0	0	0			$0.94 + 0.02\ 3s^2\ 3p^3(^2_1P)\ \ ^2P^{\circ} + 0.02\ 3s\ \ ^2S\ 3p^3(^2_3D)\ \ ^3D\ 3d\ \ ^4S^{\circ}$
26	2	$3s^2\ 3p^3(^2_3D)\ \ ^2D^{\circ}_{3/2}$	3/2−	41872	41566	306	1.84E−02	1.84E−02	$0.85 + 0.11\ 3s^2\ 3p^3(^2_1P)\ \ ^2P^{\circ}$
26	3	$3s^2\ 3p^3(^2_3D)\ \ ^2D^{\circ}_{5/2}$	5/2−	46386	46075	311	3.28E−01	3.28E−01	0.96
26	4	$3s^2\ 3p^3(^2_1P)\ \ ^2P^{\circ}_{1/2}$	1/2−	74557	74109	448	3.84E−03	3.84E−03	0.96
26	5	$3s^2\ 3p^3(^2_1P)\ \ ^2P^{\circ}_{3/2}$	3/2−	80926	80515	411	1.60E−03	1.60E−03	$0.82 + 0.11\ 3s^2\ 3p^3(^2_3D)\ \ ^2D^{\circ}$
26	6	$3s\ \ ^2S\ 3p^4(^3_2P)\ \ ^4P_{5/2}$	5/2+	274618	274373	245	6.13E−10	5.94E−10	$0.87 + 0.09\ 3s^2\ 3p^2(^3_2P)\ \ ^3P\ 3d\ \ ^4P$
26	7	$3s\ \ ^2S\ 3p^4(^3_2P)\ \ ^4P_{3/2}$	3/2+	284240	284005	235	5.68E−10	5.54E−10	$0.88 + 0.10\ 3s^2\ 3p^2(^3_2P)\ \ ^3P\ 3d\ \ ^4P$
26	8	$3s\ \ ^2S\ 3p^4(^3_2P)\ \ ^4P_{1/2}$	1/2+	288550	288307	243	5.37E−10	5.26E−10	$0.87 + 0.10\ 3s^2\ 3p^2(^3_2P)\ \ ^3P\ 3d\ \ ^4P$
26	9	$3s\ \ ^2S\ 3p^4(^1_2D)\ \ ^2D_{3/2}$	3/2+	340143	340020	123	2.73E−10	2.66E−10	$0.75 + 0.17\ 3s^2\ 3p^2(^1_2D)\ \ ^1D\ 3d\ \ ^2D + 0.03\ 3s^2\ 3p^2(^1_0S)\ \ ^1S\ 3d\ \ ^2D$
26	10	$3s\ \ ^2S\ 3p^4(^1_2D)\ \ ^2D_{5/2}$	5/2+	342090	341703	387	3.03E−10	2.94E−10	$0.76 + 0.17\ 3s^2\ 3p^2(^1_2D)\ \ ^1D\ 3d\ \ ^2D + 0.03\ 3s^2\ 3p^2(^1_0S)\ \ ^1S\ 3d\ \ ^2D$
26	11	$3s\ \ ^2S\ 3p^4(^3_2P)\ \ ^2P_{3/2}$	3/2+	389908	389706	202	1.08E−10	1.05E−10	$0.45 + 0.44\ 3s^2\ 3p^2(^3_2P)\ \ ^3P\ 3d\ \ ^2P + 0.05\ 3s^2\ 3p^2(^1_2D)\ \ ^1D\ 3d\ \ ^2P$
26	12	$3s^2\ 3p^2(^3_2P)\ \ ^3P\ 3d\ \ ^2P_{1/2}$	1/2+	394654	*394120*	534	9.66E−11	9.46E−11	$0.29 + 0.33\ 3s\ \ ^2S\ 3p^4(^3_2P)\ \ ^2P + 0.27\ 3s\ \ ^2S\ 3p^4(^1_0S)\ \ ^2S$
26	26	$3s^2\ 3p^2(^3_2P)\ \ ^3P\ 3d\ \ ^2P_{3/2}$	3/2+	502031	501800	231	1.51E−11	1.49E−11	$0.24 + 0.42\ 3s\ \ ^2S\ 3p^4(^3_2P)\ \ ^2P + 0.25\ 3s^2\ 3p^2(^1_2D)\ \ ^1D\ 3d\ \ ^2P$
26	27	$3s^2\ 3p^2(^3_2P)\ \ ^3P\ 3d\ \ ^4P_{5/2}$	5/2+	512330	512510	−180	1.19E−11	1.18E−11	$0.83 + 0.08\ 3s\ \ ^2S\ 3p^4(^3_2P)\ \ ^4P$
26	28	$3s\ \ ^2S\ 3p^4(^3_2P)\ \ ^2P_{1/2}$	1/2+	514055	513850	205	1.49E−11	1.48E−11	$0.37 + 0.30\ 3s^2\ 3p^2(^1_2D)\ \ ^1D\ 3d\ \ ^2P + 0.20\ 3s^2\ 3p^2(^3_2P)\ \ ^3P\ 3d\ \ ^2P$
26	29	$3s^2\ 3p^2(^3_2P)\ \ ^3P\ 3d\ \ ^4P_{3/2}$	3/2+	516617	516740	−123	1.17E−11	1.17E−11	$0.80 + 0.09\ 3s\ \ ^2S\ 3p^4(^3_2P)\ \ ^4P + 0.03\ 3s^2\ 3p^2(^1_0S)\ \ ^1S\ 3d\ \ ^2D$
26	30	$3s^2\ 3p^2(^3_2P)\ \ ^3P\ 3d\ \ ^4P_{1/2}$	1/2+	519641	519770	−129	1.12E−11	1.12E−11	$0.78 + 0.09\ 3s\ \ ^2S\ 3p^4(^3_2P)\ \ ^4P + 0.04\ 3s\ \ ^2S\ 3p^4(^3_2P)\ \ ^2P$
26	31	$3s^2\ 3p^2(^1_0S)\ \ ^1S\ 3d\ \ ^2D_{3/2}$	3/2+	526302	526120	182	5.62E−11	5.58E−11	$0.47 + 0.36\ 3s^2\ 3p^2(^3_2P)\ \ ^3P\ 3d\ \ ^2D + 0.05\ 3s^2\ 3p^2(^3_2P)\ \ ^3P\ 3d\ \ ^4P$
26	32	$3s^2\ 3p^2(^1_0S)\ \ ^1S\ 3d\ \ ^2D_{5/2}$	5/2+	537078	538040	−962	2.92E−11	2.90E−11	$0.41 + 0.38\ 3s^2\ 3p^2(^3_2P)\ \ ^3P\ 3d\ \ ^2D + 0.08\ 3s\ \ ^2S\ 3p^4(^1_2D)\ \ ^2D$
26	33	$3s^2\ 3p^2(^1_2D)\ \ ^1D\ 3d\ \ ^2D_{3/2}$	3/2+	554046	554030	16	1.39E−11	1.39E−11	$0.76 + 0.14\ 3s\ \ ^2S\ 3p^4(^1_2D)\ \ ^2D + 0.03\ 3s^2\ 3p^2(^1_0S)\ \ ^1S\ 3d\ \ ^2D$
26	34	$3s^2\ 3p^2(^1_2D)\ \ ^1D\ 3d\ \ ^2D_{5/2}$	5/2+	554772	554610	162	2.16E−11	2.14E−11	$0.65 + 0.20\ 3s^2\ 3p^2(^1_0S)\ \ ^1S\ 3d\ \ ^2D + 0.09\ 3s\ \ ^2S\ 3p^4(^1_2D)\ \ ^2D$
26	35	$3s^2\ 3p^2(^1_2D)\ \ ^1D\ 3d\ \ ^2P_{1/2}$	1/2+	569880	568940	940	1.47E−11	1.47E−11	$0.57 + 0.23\ 3s^2\ 3p^2(^3_2P)\ \ ^3P\ 3d\ \ ^2P + 0.09\ 3s^2\ 3p^2(^1_2D)\ \ ^1D\ 3d\ \ ^2S$
26	36	$3s^2\ 3p^2(^3_2P)\ \ ^3P\ 3d\ \ ^2F_{5/2}$	5/2+	576848	576740	108	9.62E−12	9.58E−12	$0.48 + 0.34\ 3s^2\ 3p^2(^1_2D)\ \ ^1D\ 3d\ \ ^2F + 0.08\ 3s^2\ 3p^2(^3_2P)\ \ ^3P\ 3d\ \ ^2D$
26	37	$3s^2\ 3p^2(^1_2D)\ \ ^1D\ 3d\ \ ^2P_{3/2}$	3/2+	577759	577740	19	1.44E−11	1.43E−11	$0.60 + 0.26\ 3s^2\ 3p^2(^3_2P)\ \ ^3P\ 3d\ \ ^2P + 0.05\ 3s\ \ ^2S\ 3p^4(^3_2P)\ \ ^2P$
26	38	$3s^2\ 3p^2(^1_2D)\ \ ^1D\ 3d\ \ ^2S_{1/2}$	1/2+	579837	579630	207	1.48E−11	1.46E−11	$0.69 + 0.13\ 3s\ \ ^2S\ 3p^4(^1_0S)\ \ ^2S + 0.05\ 3s^2\ 3p^2(^1_2D)\ \ ^1D\ 3d\ \ ^2P$
26	39	$3s^2\ 3p^2(^3_2P)\ \ ^3P\ 3d\ \ ^2F_{7/2}$	7/2+	581261	581180	81	9.63E−12	9.59E−12	$0.59 + 0.36\ 3s^2\ 3p^2(^1_2D)\ \ ^1D\ 3d\ \ ^2F$
26	40	$3s^2\ 3p^2(^3_2P)\ \ ^3P\ 3d\ \ ^2D_{5/2}$	5/2+	604088	603930	158	1.07E−11	1.07E−11	$0.50 + 0.25\ 3s^2\ 3p^2(^1_0S)\ \ ^1S\ 3d\ \ ^2D + 0.08\ 3s^2\ 3p^2(^3_2P)\ \ ^3P\ 3d\ \ ^2F$
26	41	$3s^2\ 3p^2(^3_2P)\ \ ^3P\ 3d\ \ ^2D_{3/2}$	3/2+	605721	605480	241	1.10E−11	1.10E−11	$0.56 + 0.36\ 3s^2\ 3p^2(^1_0S)\ \ ^1S\ 3d\ \ ^2D$
26	272	$3s^2\ 3p^2(^3_2P)\ \ ^3P\ 4s\ \ ^4P_{1/2}$	1/2+	1242245	1242000	245	1.27E−11	1.27E−11	$0.65 + 0.14\ 3s\ \ ^2S\ 3p^2(^3_2P)\ \ ^4P\ 3d^2(^1_0S)\ \ ^4P + 0.06\ 3s^2\ 3p^2(^3_2P)\ \ ^3P\ 4s\ \ ^2P$
26	282	$3s^2\ 3p^2(^3_2P)\ \ ^3P\ 4s\ \ ^4P_{3/2}$	3/2+	1249844	1249660	184	1.36E−11	1.36E−11	$0.72 + 0.11\ 3s\ \ ^2S\ 3p^2(^3_2P)\ \ ^4P\ 3d^2(^1_0S)\ \ ^4P + 0.03\ 3s\ \ ^2S\ 3p^2(^1_0S)\ \ ^2S\ 3d^2(^3_2P)\ \ ^4P$
26	291	$3s^2\ 3p^2(^3_2P)\ \ ^3P\ 4s\ \ ^2P_{1/2}$	1/2+	1257717	1257730	−13	4.34E−12	4.35E−12	$0.86 + 0.06\ 3s^2\ 3p^2(^3_2P)\ \ ^3P\ 4s\ \ ^4P$
26	292	$3s^2\ 3p^2(^3_2P)\ \ ^3P\ 4s\ \ ^4P_{5/2}$	5/2+	1258123	1258050	73	1.39E−11	1.38E−11	$0.72 + 0.10\ 3s\ \ ^2S\ 3p^2(^3_2P)\ \ ^4P\ 3d^2(^1_0S)\ \ ^4P + 0.06\ 3s^2\ 3p^2(^1_2D)\ \ ^1D\ 4s\ \ ^2D$
26	297	$3s^2\ 3p^2(^3_2P)\ \ ^3P\ 4s\ \ ^2P_{3/2}$	3/2+	1266649	1266360	289	4.84E−12	4.85E−12	$0.69 + 0.14\ 3s^2\ 3p^2(^1_2D)\ \ ^1D\ 4s\ \ ^2D + 0.06\ 3s\ \ ^2S\ 3p^2(^3_2P)\ \ ^4P\ 3d^2(^3_2P)\ \ ^4S$
26	327	$3s^2\ 3p^2(^1_2D)\ \ ^1D\ 4s\ \ ^2D_{5/2}$	5/2+	1287928	1287700	228	8.68E−12	8.67E−12	$0.62 + 0.05\ 3s^2\ 3p^2(^3_2P)\ \ ^3P\ 4s\ \ ^4P + 0.04\ 3s\ \ ^2S\ 3p^2(^1_2D)\ \ ^2D\ 3d^2(^1_2G)\ \ ^2F$
26	328	$3s^2\ 3p^2(^1_2D)\ \ ^1D\ 4s\ \ ^2D_{3/2}$	3/2+	1289213	1289060	153	6.83E−12	6.84E−12	$0.71 + 0.12\ 3s^2\ 3p^2(^3_2P)\ \ ^3P\ 4s\ \ ^2P + 0.03\ 3s\ \ ^2S\ 3p^2(^3_2P)\ \ ^2P\ 3d^2(^1_2D)\ \ ^2D$
26	488	$3s^2\ 3p^2(^3_2P)\ \ ^3P\ 4d\ \ ^4P_{5/2}$	5/2+	1507751	1508360	−609	6.20E−12	6.16E−12	$0.21 + 0.30\ 3s^2\ 3d^3(^2_3F)\ \ ^2F + 0.14\ 3s^2\ 3p^2(^3_2P)\ \ ^3P\ 4d\ \ ^4F$
26	493	$3s^2\ 3p^2(^3_2P)\ \ ^3P\ 4d\ \ ^4F_{5/2}$	5/2+	1514177	1514070	107	7.30E−12	7.23E−12	$0.52 + 0.37\ 3s^2\ 3p^2(^3_2P)\ \ ^3P\ 4d\ \ ^4P + 0.04\ 3s^2\ 3p^2(^3_2P)\ \ ^3P\ 4d\ \ ^2F$
26	496	$3s^2\ 3p^2(^3_2P)\ \ ^3P\ 4d\ \ ^4P_{3/2}$	3/2+	1517434	1517340	94	4.22E−12	4.17E−12	$0.67 + 0.16\ 3s^2\ 3p^2(^3_2P)\ \ ^3P\ 4d\ \ ^2P + 0.06\ 3s^2\ 3p^2(^3_2P)\ \ ^3P\ 4d\ \ ^4D$
26	498	$3s^2\ 3p^2(^3_2P)\ \ ^3P\ 4d\ \ ^2F_{5/2}$	5/2+	1518836	1516030	**2806**	7.13E−12	7.05E−12	$0.70 + 0.12\ 3s^2\ 3p^2(^3_2P)\ \ ^3P\ 4d\ \ ^4F + 0.06\ 3s^2\ 3p^2(^1_2D)\ \ ^1D\ 4d\ \ ^2F$
26	507	$3s^2\ 3p^2(^3_2P)\ \ ^3P\ 4d\ \ ^2F_{7/2}$	7/2+	1526756	1523140	**3616**	1.32E−11	1.31E−11	$0.52 + 0.18\ 3s^2\ 3p^2(^3_2P)\ \ ^3P\ 4d\ \ ^4D + 0.10\ 3s^2\ 3p^2(^3_2P)\ \ ^3P\ 4d\ \ ^4F$
26	520	$3s^2\ 3p^2(^3_2P)\ \ ^3P\ 4d\ \ ^4D_{7/2}$	7/2+	1532429	1532160	269	5.12E−12	5.07E−12	$0.50 + 0.30\ 3s^2\ 3p^2(^3_2P)\ \ ^3P\ 4d\ \ ^2F + 0.11\ 3s^2\ 3p^2(^1_2D)\ \ ^1D\ 4d\ \ ^2F$

Table 2
(Continued)

Z	Key	Level	$J\pi$	$E_{\rm MCDHF}$	$E_{\rm NIST}$	ΔE	$\tau^{l}_{\rm MCDHF}$	$\tau^{v}_{\rm MCDHF}$	LS-composition
26	525	$3s^2\ 3p^2(^3_2P)\ ^3P\ 4d\ ^2D_{5/2}$	5/2+	1535024	1534990	34	4.27E−12	4.22E−12	$0.63 + 0.24\ 3s^2\ 3p^2(^1_2D)\ ^1D\ 4d\ ^2F + 0.05\ 3s^2\ 3p^2(^1_2D)\ ^1D\ 4d\ ^2D$
26	528	$3s^2\ 3p^2(^3_2P)\ ^3P\ 4d\ ^2D_{3/2}$	3/2+	1536959	1536480	479	4.18E−12	4.12E−12	$0.78 + 0.05\ 3s^2\ 3p^2(^1_2D)\ ^1D\ 4d\ ^2D + 0.03\ 3s^2\ 3p^2(^3_2P)\ ^3P\ 4d\ ^2P$
26	542	$3s^2\ 3p^2(^1_2D)\ ^1D\ 4d\ ^2F_{7/2}$	7/2+	1549492	1549250	242	6.95E−12	6.90E−12	$0.73 + 0.16\ 3s^2\ 3p^2(^3_2P)\ ^3P\ 4d\ ^4D + 0.03\ 3s^2\ 3p^2(^3_2P)\ ^3P\ 4d\ ^4F$
26	545	$3s^2\ 3p^2(^1_2D)\ ^1D\ 4d\ ^2F_{5/2}$	5/2+	1550449	1551400	−951	4.48E−12	4.44E−12	$0.41 + 0.30\ 3s^2\ 3p^2(^1_2D)\ ^1D\ 4d\ ^2D + 0.07\ 3s^2\ 3p^2(^3_2P)\ ^3P\ 4d\ ^4D$
26	552	$3s^2\ 3p^2(^1_2D)\ ^1D\ 4d\ ^2D_{5/2}$	5/2+	1555381	1551640	**3741**	3.21E−12	3.17E−12	$0.40 + 0.21\ 3s^2\ 3p^2(^3_2P)\ ^3P\ 4d\ ^2D + 0.16\ 3s^2\ 3p^2(^1_2D)\ ^1D\ 4d\ ^2F$
26	570	$3s^2\ 3p^2(^1_2D)\ ^1D\ 4d\ ^2P_{3/2}$	3/2+	1566331	1565720	611	5.05E−12	4.96E−12	$0.87 + 0.02\ 3s^2\ 3p^2(^3_2P)\ ^3P\ 4d\ ^4P$
26	581	$3s^2\ 3p^2(^1_2D)\ ^1D\ 4d\ ^2S_{1/2}$	1/2+	1574583	1569410	**5173**	6.67E−12	6.58E−12	0.89
27	1	$3s^2\ 3p^3(^4_3S)\ ^4S^\circ_{3/2}$	3/2−	0	0	0			$0.93 + 0.03\ 3s^2\ 3p^3(^2_1P)\ ^2P^\circ + 0.02\ 3s\ ^2S\ 3p^3(^2_3D)\ ^3D\ 3d\ ^4S^\circ$
27	2	$3s^2\ 3p^3(^2_3D)\ ^2D^\circ_{3/2}$	3/2−	43985	43650	335	9.84E−03	9.84E−03	$0.83 + 0.12\ 3s^2\ 3p^3(^2_1P)\ ^2P^\circ$
27	3	$3s^2\ 3p^3(^2_3D)\ ^2D^\circ_{5/2}$	5/2−	49988	49690	298	1.50E−01	1.50E−01	0.97
27	4	$3s^2\ 3p^3(^2_1P)\ ^2P^\circ_{1/2}$	1/2−	79931	79460	471	2.38E−03	2.39E−03	0.96
27	5	$3s^2\ 3p^3(^2_1P)\ ^2P^\circ_{3/2}$	3/2−	88576	88170	406	9.94E−04	9.95E−04	$0.80 + 0.13\ 3s^2\ 3p^3(^2_3D)\ ^2D^\circ + 0.02\ 3s^2\ 3p^3(^4_3S)\ ^4S^\circ$
27	6	$3s\ ^2S\ 3p^4(^3_2P)\ ^4P_{5/2}$	5/2+	295345	295160	185	5.39E−10	5.22E−10	$0.87 + 0.09\ 3s^2\ 3p^2(^3_2P)\ ^3P\ 3d\ ^4P$
27	7	$3s\ ^2S\ 3p^4(^3_2P)\ ^4P_{3/2}$	3/2+	307216	307030	186	4.93E−10	4.81E−10	$0.88 + 0.09\ 3s^2\ 3p^2(^3_2P)\ ^3P\ 3d\ ^4P$
27	8	$3s\ ^2S\ 3p^4(^3_2P)\ ^4P_{1/2}$	1/2+	312302	312110	192	4.62E−10	4.53E−10	$0.87 + 0.10\ 3s^2\ 3p^2(^3_2P)\ ^3P\ 3d\ ^4P$
27	9	$3s\ ^2S\ 3p^4(^1_2D)\ ^2D_{3/2}$	3/2+	365890	365530	360	2.37E−10	2.31E−10	$0.75 + 0.16\ 3s^2\ 3p^2(^1_2D)\ ^1D\ 3d\ ^2D + 0.03\ 3s^2\ 3p^2(^1_0S)\ ^1S\ 3d\ ^2D$
27	10	$3s\ ^2S\ 3p^4(^1_2D)\ ^2D_{5/2}$	5/2+	368568	368250	318	2.67E−10	2.59E−10	$0.76 + 0.17\ 3s^2\ 3p^2(^1_2D)\ ^1D\ 3d\ ^2D + 0.03\ 3s^2\ 3p^2(^1_0S)\ ^1S\ 3d\ ^2D$
27	11	$3s\ ^2S\ 3p^4(^3_2P)\ ^2P_{3/2}$	3/2+	418617	418480	137	9.67E−11	9.46E−11	$0.45 + 0.44\ 3s^2\ 3p^2(^3_2P)\ ^3P\ 3d\ ^2P + 0.05\ 3s^2\ 3p^2(^1_2D)\ ^1D\ 3d\ ^2P$
27	12	$3s^2\ 3p^2(^3_2P)\ ^3P\ 3d\ ^2P_{1/2}$	1/2+	423634	*423290*	344	8.49E−11	8.32E−11	$0.27 + 0.31\ 3s\ ^2S\ 3p^4(^3_2P)\ ^2P + 0.30\ 3s\ ^2S\ 3p^4(^1_0S)\ ^2S$
27	27	$3s^2\ 3p^2(^3_2P)\ ^3P\ 3d\ ^4P_{5/2}$	5/2+	547650	547890	−240	1.11E−11	1.10E−11	$0.82 + 0.08\ 3s\ ^2S\ 3p^4(^3_2P)\ ^4P + 0.02\ 3s^2\ 3p^2(^1_0S)\ ^1S\ 3d\ ^2D$
27	29	$3s^2\ 3p^2(^3_2P)\ ^3P\ 3d\ ^4P_{3/2}$	3/2+	552688	552880	−192	1.10E−11	1.10E−11	$0.78 + 0.08\ 3s\ ^2S\ 3p^4(^3_2P)\ ^4P + 0.03\ 3s^2\ 3p^2(^1_0S)\ ^1S\ 3d\ ^2D$
27	30	$3s^2\ 3p^2(^3_2P)\ ^3P\ 3d\ ^4P_{1/2}$	1/2+	556693	556820	−127	1.05E−11	1.04E−11	$0.72 + 0.08\ 3s\ ^2S\ 3p^4(^3_2P)\ ^4P + 0.07\ 3s\ ^2S\ 3p^4(^3_2P)\ ^2P$
27	33	$3s^2\ 3p^2(^1_2D)\ ^1D\ 3d\ ^2D_{3/2}$	3/2+	592920	592830	90	1.28E−11	1.27E−11	$0.76 + 0.14\ 3s\ ^2S\ 3p^4(^1_2D)\ ^2D + 0.03\ 3s^2\ 3p^2(^1_0S)\ ^1S\ 3d\ ^2D$
27	34	$3s^2\ 3p^2(^1_2D)\ ^1D\ 3d\ ^2D_{5/2}$	5/2+	594302	594200	102	2.21E−11	2.19E−11	$0.62 + 0.24\ 3s^2\ 3p^2(^1_0S)\ ^1S\ 3d\ ^2D + 0.08\ 3s\ ^2S\ 3p^4(^1_2D)\ ^2D$
27	35	$3s^2\ 3p^2(^1_2D)\ ^1D\ 3d\ ^2P_{1/2}$	1/2+	608977	608870	107	1.38E−11	1.37E−11	$0.57 + 0.22\ 3s^2\ 3p^2(^3_2P)\ ^3P\ 3d\ ^2P + 0.10\ 3s^2\ 3p^2(^1_2D)\ ^1D\ 3d\ ^2S$
27	37	$3s^2\ 3p^2(^1_2D)\ ^1D\ 3d\ ^2P_{3/2}$	3/2+	618896	618880	16	1.33E−11	1.33E−11	$0.60 + 0.26\ 3s^2\ 3p^2(^3_2P)\ ^3P\ 3d\ ^2P + 0.05\ 3s\ ^2S\ 3p^4(^3_2P)\ ^2P$
27	39	$3s^2\ 3p^2(^3_2P)\ ^3P\ 3d\ ^2F_{7/2}$	7/2+	621687	621710	−23	9.00E−12	8.97E−12	$0.60 + 0.36\ 3s^2\ 3p^2(^1_2D)\ ^1D\ 3d\ ^2F$
27	40	$3s^2\ 3p^2(^3_2P)\ ^3P\ 3d\ ^2D_{5/2}$	5/2+	646974	646890	84	1.00E−11	9.99E−12	$0.48 + 0.24\ 3s^2\ 3p^2(^1_0S)\ ^1S\ 3d\ ^2D + 0.10\ 3s^2\ 3p^2(^3_2P)\ ^3P\ 3d\ ^2F$
27	41	$3s^2\ 3p^2(^3_2P)\ ^3P\ 3d\ ^2D_{3/2}$	3/2+	648502	648390	112	1.03E−11	1.03E−11	$0.56 + 0.37\ 3s^2\ 3p^2(^1_0S)\ ^1S\ 3d\ ^2D$
27	354	$3s^2\ 3p^2(^3_2P)\ ^3P\ 4s\ ^4P_{5/2}$	5/2+	1431966	*1432000*	−34	9.71E−12	9.67E−12	$0.44 + 0.13\ 3s\ ^2S\ 3p^2(^1_0S)\ ^2S\ 3d^2(^3_2P)\ ^4P + 0.07\ 3s\ ^2S\ 3p^2(^3_2P)\ ^2P\ 3d^2(^3_2P)\ ^4D$
27	355	$3s^2\ 3p^2(^3_2P)\ ^3P\ 4s\ ^2P_{1/2}$	1/2+	1432716	*1432200*	516	4.83E−12	4.82E−12	$0.40 + 0.16\ 3s\ ^2S\ 3p^2(^3_2P)\ ^2P\ 3d^2(^1_2D)\ ^2P + 0.15\ 3s\ ^2S\ 3p^2(^1_2D)\ ^2D\ 3d^2(^3_2P)\ ^2P$
27	363	$3s^2\ 3p^2(^3_2P)\ ^3P\ 4s\ ^2P_{3/2}$	3/2+	1441639	*1441700*	−61	4.16E−12	4.16E−12	$0.57 + 0.11\ 3s^2\ 3p^2(^1_2D)\ ^1D\ 4s\ ^2D + 0.03\ 3s\ ^2S\ 3p^2(^3_2P)\ ^2P\ 3d^2(^1_2D)\ ^2P$
27	378	$3s^2\ 3p^2(^1_2D)\ ^1D\ 4s\ ^2D_{5/2}$	5/2+	1464096	*1464500*	−404	6.30E−12	6.29E−12	$0.59 + 0.11\ 3s\ ^2S\ 3p^2(^3_2P)\ ^2P\ 3d^2(^3_2P)\ ^4P + 0.06\ 3s^2\ 3p^2(^3_2P)\ ^3P\ 4s\ ^4P$
27	569	$3s^2\ 3p^2(^3_2P)\ ^3P\ 4d\ ^2F_{5/2}$	5/2+	1714631	1710600	**4031**	5.16E−12	5.11E−12	$0.68 + 0.14\ 3s^2\ 3p^2(^3_2P)\ ^3P\ 4d\ ^4F + 0.06\ 3s^2\ 3p^2(^1_2D)\ ^1D\ 4d\ ^2F$
27	584	$3s^2\ 3p^2(^3_2P)\ ^3P\ 4d\ ^2F_{7/2}$	7/2+	1723923	1720300	**3623**	1.15E−11	1.14E−11	$0.48 + 0.19\ 3s^2\ 3p^2(^3_2P)\ ^3P\ 4d\ ^4D + 0.11\ 3s^2\ 3p^2(^3_2P)\ ^3P\ 4d\ ^4F$
27	593	$3s^2\ 3p^2(^3_2P)\ ^3P\ 4d\ ^4D_{7/2}$	7/2+	1730080	1729500	580	3.19E−12	3.15E−12	$0.44 + 0.33\ 3s^2\ 3p^2(^3_2P)\ ^3P\ 4d\ ^2F + 0.14\ 3s^2\ 3p^2(^1_2D)\ ^1D\ 4d\ ^2F$
27	601	$3s^2\ 3p^2(^3_2P)\ ^3P\ 4d\ ^2D_{3/2}$	3/2+	1735374	1466300	**269074**	2.94E−12	2.90E−12	$0.78 + 0.07\ 3s^2\ 3p^2(^1_2D)\ ^1D\ 4d\ ^2D + 0.03\ 3s^2\ 3p^2(^3_2P)\ ^3P\ 4d\ ^2P$
27	641	$3s^2\ 3p^2(^1_2D)\ ^1D\ 4d\ ^2D_{5/2}$	5/2+	1755567	1751800	**3767**	2.17E−12	2.14E−12	$0.38 + 0.24\ 3s^2\ 3p^2(^3_2P)\ ^3P\ 4d\ ^2D + 0.20\ 3s^2\ 3p^2(^1_2D)\ ^1D\ 4d\ ^2F$
28	1	$3s^2\ 3p^3(^4_3S)\ ^4S^\circ_{3/2}$	3/2−	0	0	0			$0.92 + 0.04\ 3s^2\ 3p^3(^2_1P)\ ^2P^\circ$
28	2	$3s^2\ 3p^3(^2_3D)\ ^2D^\circ_{3/2}$	3/2−	45966	45767.8	198.2	5.51E−03	5.51E−03	$0.81 + 0.14\ 3s^2\ 3p^3(^2_1P)\ ^2P^\circ + 0.02\ 3s^2\ 3p^3(^4_3S)\ ^4S^\circ$
28	3	$3s^2\ 3p^3(^2_3D)\ ^2D^\circ_{5/2}$	5/2−	53763	53569	194	7.20E−02	7.20E−02	0.97
28	4	$3s^2\ 3p^3(^2_1P)\ ^2P^\circ_{1/2}$	1/2−	85411	85126.7	284.3	1.51E−03	1.51E−03	0.96

Table 2
(Continued)

Z	Key	Level	$J\pi$	$E_{\rm MCDHF}$	$E_{\rm NIST}$	ΔE	$\tau^{l}_{\rm MCDHF}$	$\tau^{v}_{\rm MCDHF}$	LS-composition
28	5	$3s^2\ 3p^3(^2_1P)\ ^2P^{\circ}_{3/2}$	3/2−	96917	96630	287	6.31E−04	6.31E−04	$0.78 + 0.15\ 3s^2\ 3p^3(^2_3D)\ ^2D^{\circ} + 0.03\ 3s^2\ 3p^3(^4_3S)\ ^4S^{\circ}$
28	6	$3s\ ^2S\ 3p^4(^3_2P)\ ^4P_{5/2}$	5/2+	316289	316343	−54	4.79E−10	4.62E−10	$0.87 + 0.09\ 3s^2\ 3p^2(^3_2P)\ ^3P\ 3d\ ^4P$
28	7	$3s\ ^2S\ 3p^4(^3_2P)\ ^4P_{3/2}$	3/2+	330776	330837	−61	4.32E−10	4.20E−10	$0.87 + 0.09\ 3s^2\ 3p^2(^3_2P)\ ^3P\ 3d\ ^4P$
28	9	$3s\ ^2S\ 3p^4(^1_2D)\ ^2D_{3/2}$	3/2+	392010	391916	94	2.07E−10	2.02E−10	$0.74 + 0.16\ 3s^2\ 3p^2(^1_2D)\ ^1D\ 3d\ ^2D + 0.03\ 3s^2\ 3p^2(^1_0S)\ ^1S\ 3d\ ^2D$
28	10	$3s\ ^2S\ 3p^4(^1_2D)\ ^2D_{5/2}$	5/2+	395637	395567	70	2.38E−10	2.31E−10	$0.76 + 0.17\ 3s^2\ 3p^2(^1_2D)\ ^1D\ 3d\ ^2D + 0.03\ 3s^2\ 3p^2(^1_0S)\ ^1S\ 3d\ ^2D$
28	11	$3s\ ^2S\ 3p^4(^3_2P)\ ^2P_{3/2}$	3/2+	447660	447765	−105	8.83E−11	8.63E−11	$0.44 + 0.44\ 3s^2\ 3p^2(^3_2P)\ ^3P\ 3d\ ^2P + 0.05\ 3s^2\ 3p^2(^1_2D)\ ^1D\ 3d\ ^2P$
28	12	$3s\ ^2S\ 3p^4(^3_2P)\ ^2P_{1/2}$	1/2+	452920	452850	70	7.55E−11	7.38E−11	$0.30 + 0.32\ 3s\ ^2S\ 3p^4(^1_0S)\ ^2S + 0.25\ 3s^2\ 3p^2(^3_2P)\ ^3P\ 3d\ ^2P$
28	27	$3s^2\ 3p^2(^3_2P)\ ^3P\ 3d\ ^4P_{5/2}$	5/2+	583004	583530	−526	1.04E−11	1.03E−11	$0.81 + 0.08\ 3s\ ^2S\ 3p^4(^3_2P)\ ^4P + 0.02\ 3s^2\ 3p^2(^1_0S)\ ^1S\ 3d\ ^2D$
28	29	$3s^2\ 3p^2(^3_2P)\ ^3P\ 3d\ ^4P_{3/2}$	3/2+	588832	589310	−478	1.04E−11	1.04E−11	$0.76 + 0.08\ 3s\ ^2S\ 3p^4(^3_2P)\ ^4P + 0.04\ 3s^2\ 3p^2(^1_0S)\ ^1S\ 3d\ ^2D$
28	30	$3s^2\ 3p^2(^3_2P)\ ^3P\ 3d\ ^4P_{1/2}$	1/2+	594316	594810	−494	9.99E−12	9.91E−12	$0.60 + 0.13\ 3s\ ^2S\ 3p^4(^3_2P)\ ^2P + 0.09\ 3s^2\ 3p^2(^3_2P)\ ^3P\ 3d\ ^2P$
28	33	$3s^2\ 3p^2(^1_2D)\ ^1D\ 3d\ ^2D_{3/2}$	3/2+	632033	632280	−247	1.17E−11	1.16E−11	$0.75 + 0.14\ 3s\ ^2S\ 3p^4(^1_2D)\ ^2D + 0.02\ 3s^2\ 3p^2(^1_0S)\ ^1S\ 3d\ ^2D$
28	34	$3s^2\ 3p^2(^1_2D)\ ^1D\ 3d\ ^2D_{5/2}$	5/2+	634264	634430	−166	2.31E−11	2.30E−11	$0.59 + 0.28\ 3s^2\ 3p^2(^1_0S)\ ^1S\ 3d\ ^2D + 0.06\ 3s\ ^2S\ 3p^4(^1_2D)\ ^2D$
28	35	$3s^2\ 3p^2(^1_2D)\ ^1D\ 3d\ ^2P_{1/2}$	1/2+	648108	648320	−212	1.29E−11	1.29E−11	$0.57 + 0.22\ 3s^2\ 3p^2(^3_2P)\ ^3P\ 3d\ ^2P + 0.10\ 3s^2\ 3p^2(^1_2D)\ ^1D\ 3d\ ^2S$
28	37	$3s^2\ 3p^2(^1_2D)\ ^1D\ 3d\ ^2P_{3/2}$	3/2+	660460	660710	−250	1.25E−11	1.24E−11	$0.59 + 0.26\ 3s^2\ 3p^2(^3_2P)\ ^3P\ 3d\ ^2P + 0.05\ 3s\ ^2S\ 3p^4(^3_2P)\ ^2P$
28	38	$3s^2\ 3p^2(^3_2P)\ ^3P\ 3d\ ^2F_{7/2}$	7/2+	662315	662780	−465	8.46E−12	8.43E−12	$0.60 + 0.35\ 3s^2\ 3p^2(^1_2D)\ ^1D\ 3d\ ^2F$
28	40	$3s^2\ 3p^2(^3_2P)\ ^3P\ 3d\ ^2D_{5/2}$	5/2+	690353	690560	−207	9.41E−12	9.37E−12	$0.47 + 0.24\ 3s^2\ 3p^2(^1_0S)\ ^1S\ 3d\ ^2D + 0.11\ 3s^2\ 3p^2(^3_2P)\ ^3P\ 3d\ ^2F$
28	41	$3s^2\ 3p^2(^3_2P)\ ^3P\ 3d\ ^2D_{3/2}$	3/2+	691654	691930	−276	9.72E−12	9.68E−12	$0.56 + 0.37\ 3s^2\ 3p^2(^1_0S)\ ^1S\ 3d\ ^2D$
28	638	$3s^2\ 3p^2(^3_2P)\ ^3P\ 4d\ ^2P_{3/2}$	3/2+	1914451	1628400	**286051**	5.35E−12	5.31E−12	$0.42 + 0.40\ 3s^2\ 3p^2(^3_2P)\ ^3P\ 4d\ ^4F + 0.10\ 3s^2\ 3p^2(^3_2P)\ ^3P\ 4d\ ^4P$
28	674	$3s^2\ 3p^2(^3_2P)\ ^3P\ 4d\ ^2D_{5/2}$	5/2+	1940510	1653100	**287410**	2.27E−12	2.25E−12	$0.56 + 0.28\ 3s^2\ 3p^2(^1_2D)\ ^1D\ 4d\ ^2F + 0.08\ 3s^2\ 3p^2(^1_2D)\ ^1D\ 4d\ ^2D$

Note. $E_{\rm MCDHF}$: our MCDHF excitation energies. $E_{\rm NIST}$: observed values compiled in the NIST ASD (Kramida et al. 2018). ΔE: energy differences (in $\rm cm^{-1}$) between the values of $E_{\rm MCDHF}$ and $E_{\rm NIST}$. $\tau^{l}_{\rm MCDHF}$: our MCDHF lifetimes in length form. $\tau^{v}_{\rm MCDHF}$: our MCDHF lifetimes in velocity form. LS-composition: the LS eigenvector compositions. Many levels are strongly mixed, implying ambiguous configuration labels. In these cases, the parity, J, and energy are used to match the theoretical levels with the atomic energy levels from NIST ASD. For those levels, the NIST values are shown in the italics. Energy differences larger than 2000 $\rm cm^{-1}$ are displayed in bold. The results for the levels, for which the NIST values are available, are shown here for guidance regarding its form and content.

(This table is available in its entirety in machine-readable form.)

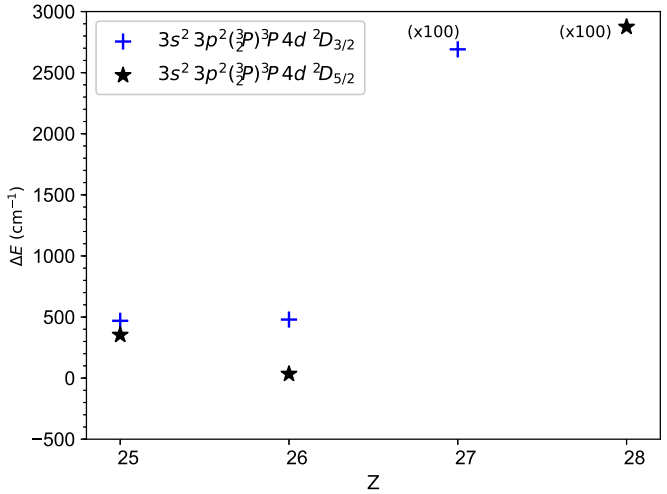

Figure 1. Energy differences, ΔE (in cm^{-1}), between E_{MCDHF} and E_{NIST} are displayed as a function of the nuclear charge Z for the $3s^2\ 3p^2(^3_2P)\ ^3P\ 4d\ ^2D_{3/2}$ and $3s^2\ 3p^2(^3_2P)\ ^3P\ 4d\ ^2D_{5/2}$ states. The corresponding data are available in Table 2. The real differences for the $3s^2\ 3p^2(^3_2P)\ ^3P\ 4d\ ^2D_{3/2}$ state in Co XIII ($Z = 27$) and $3s^2\ 3p^2(^3_2P)\ ^3P\ 4d\ ^2D_{5/2}$ state in Ni XIV ($Z = 28$) are reduced by a factor of 100, as marked by the ($\times$100) label.

misprint, the average absolute differences with our MCDHF1 energy values are $-164 \pm 313\ cm^{-1}$ for NIST and $-113 \pm 313\ cm^{-1}$ for CHIANTI1, respectively, where the standard deviations are indicated after the values.

Looking at higher-lying levels (above #143) in Fe XII, the present MCDHF1 calculations, as well as the CHIANTI2 theoretical values reported by the AUTOSTRUCTURE calculations by Del Zanna et al. (2012b), provide a complete data set. The AUTOSTRUCTURE calculations were carried out to provide target state wave functions for the scattering calculations. They are therefore not very accurate, providing excitation energies that indeed depart substantially from the present MCDHF1 values. For almost all higher-lying states of Fe XII, experimental values (NIST and CHIANTI1) are scarce. Only some levels of the $3s^23p^24s$, $3s^23p^24p$, $3s^23p^24d$, and $3s3p^34s$ were identified, based on the solar and laboratory spectra of Behring et al. (1972) and Fawcett et al. (1972). The differences between our MCDHF1 excitation energies and the experimental values (NIST and CHIANTI1) are generally within a few hundreds of cm^{-1}. However, several discrepancies have been noted, as described below.

Our MCDHF excitation energies, E_{MCDHF} (cm^{-1}), together with MCDHF radiative lifetimes, τ^l_{MCDHF} (in s), in the length form and τ^v_{MCDHF} (in s) in the velocity form are reported in Table 2 for the lowest 546 (623, 701, and 745) states of the $3p^43d, 3s3p^23d^2, 3s3p^34p, 3s3p^4, 3s^23d^3, 3s^23p^23d, 3s^23p^24d, 3s^23p^24s, 3p^33d^2, 3p^5, 3s3p3d^3, 3s3p^33d, 3s3p^34s, 3s^23p3d^2, 3s^23p^24p$, and $3s^23p^3$ configurations in Mn XI (Fe XII, Co XIII, and Ni XIV). Observed values E_{NIST} (cm^{-1}) from the NIST ASD (Kramida et al. 2018) and energy differences ΔE (cm^{-1}) between the values of E_{MCDHF} and E_{NIST} are also listed in this table. As many levels are strongly mixed, their configuration label is not unique. Here, the parity, J value, and energy are used to match the levels to the NIST ASD. For those levels, the NIST values are shown in italics. The experimental excitation energies E_{NIST} agree well with our E_{MCDHF} values for a majority of the $n = 4$ states. However, there are 14 levels, including 4 levels in Mn XI, 4 levels in Fe XII, 4 levels in Co XIII, and 2 levels in Ni XIV, for which differences are over $2000\ cm^{-1}$. The $3s^2\ 3p^2(^3_2P)\ ^3P\ 4d\ ^2F_{7/2}$ state in Fe XII, where E_{NIST} and E_{MCDHF} differ by $3616\ cm^{-1}$, is discussed below in detail. For the same levels, large difference of about $3700\ cm^{-1}$ also occur for Mn XI and Co XIII. As an example, the energy differences ΔE between E_{MCDHF} and E_{NIST} as a function of the nuclear charge Z are displayed in Figure 1 for the $3s^2\ 3p^2(^3_2P)\ ^3P\ 4d\ ^2D_{3/2}$ and $3s^2\ 3p^2(^3_2P)\ ^3P\ 4d\ ^2D_{5/2}$ states. Two anomalies appear for the $3s^2\ 3p^2(^3_2P)\ ^3P\ 4d\ ^2D_{3/2}$ state in Co XIII and the $3s^2\ 3p^2(^3_2P)\ ^3P\ 4d\ ^2D_{5/2}$ state in Ni XIV. Since the same MCDHF computational processes are carried out for all the ions, the accuracy of our MCDHF excitation energies along the sequence should be systematic and consistency is expected. Therefore, the large differences indicate that the identifications involving these levels are questionable or that the wavelengths are incorrect.

3.2. Fe XII Line Identifications

In this section, we review the identifications of the main Fe XII transitions $n = 4 \rightarrow n = 3$ transitions. While Del Zanna et al. (2012b) only considered the strongest transitions at low plasma density (10^8 electrons cm^{-3}), here we consider the strongest transitions at high plasma density (10^{19} electrons cm^{-3}) to review Fawcett's identifications based on the laboratory plates. We have also considered one of Fawcett's plates for the evaluation. Table 3 lists the strongest $n = 4 \rightarrow n = 3$ transitions in Fe XII, calculated with the atomic data described in Del Zanna et al. (2012b). In addition to Fawcett's wavelengths, we list the approximate AUTOSTRUCTURE values and our MCDHF wavelengths, with several comments. Spectral lines that are strongest in low plasma density are noted with an asterisk.

For the strongest lines of the $3s^23p^23d$–$3s^23p^24p$ transition array, we find a good agreement (within 0.05 Å) between Fawcett's wavelengths and our predicted values. There are some important transitions visible at low densities, from the $\#392/3s^2\ 3p^2(^3_2P)\ ^3P\ 4p\ ^4S^o_{3/2}$ level. Our values are in excellent agreement (0.009 Å) with the identifications proposed by Del Zanna (2012b). Generally, we confirm the CHIANTI1 experimental excitation energies for the $3s^23p^24p$ levels (#371, #380, #387, #392, #407, and #408), proposed by Del Zanna (2012b), as the differences with our MCDHF1 are around a few hundreds cm^{-1}. However, for level $\#387/3s^2\ 3p^2(^3_2P)\ ^3P4p\ ^4D^o_{7/2}$, the difference is larger ($-5252\ cm^{-1}$). The original assignment by Fawcett et al. (1972) of the line at 108.44 Å value to the transition $3s^2\ 3p^2(^3_2P)\ ^3P\ 4p\ ^4D^o_{7/2}$–$3s^2\ 3p^2(^3_2P)\ ^3P\ 3d\ ^4F_{9/2}$ is most likely correct. Using the CHIANTI1 experimental excitation energy 443,121 cm^{-1} for the lower level, this results in an energy of 1,365,290 cm^{-1} for the upper level, which is in good agreement with our MCDHF1 result (1,365,552 cm^{-1}).

Regarding the $3s^23p^3$–$3s^23p^24s$ transition array, very good agreement with Fawcett's values is observed. The differences of our MCDHF1 excitation energies and experimental values (NIST and CHIANTI1) for the $3s^23p^24s$ levels are within $300\ cm^{-1}$.

We also confirm the identifications proposed by Del Zanna (2012b) of the decays from the $\#471/3s\ ^2S\ 3p^3(^4_3S)\ ^5S\ 4s\ ^4S^o_{3/2}$ level, which are the strongest Fe XII transitions at low astrophysical densities. In Del Zanna (2012b), the 83.336 and 83.631 Å lines observed by Behring et al. (1972) were tentatively assigned to the decays from level $\#471/3s\ ^2S\ 3p^3(^4_3S)\ ^5S\ 4s\ ^4S^o_{3/2}$ to the lower levels $\#7/3s\ ^2S\ 3p^4(^3_2P)\ ^4P_{3/2}$ and

Table 3
A List of the Strongest Lines from $n = 4$ Levels for Fe XII

i–j	Transition	Int	λ_{exp}	λ_{AS}	λ_{MCDHF}	λ_{rev}	Notes
18–387	$3s^2\ 3p^2(^3_2P)\ ^3P\ 3d\ ^4F_{9/2}$–$3s^2\ 3p^2(^3_2P)\ ^3P\ 4p\ ^4D^o_{7/2}$	1.2	108.440	107.04	108.38 (−0.06)		
25–408	$3s^2\ 3p^2(^1_2D)\ ^1D\ 3d\ ^2G_{9/2}$–$3s^2\ 3p^2(^1_2D)\ ^1D\ 4p\ ^2F^o_{7/2}$	1.1	110.591	109.20	110.527 (−0.06)		
16–380	$3s^2\ 3p^2(^3_2P)\ ^3P\ 3d\ ^4F_{7/2}$–$3s^2\ 3p^2(^3_2P)\ ^3P\ 4p\ ^4D^o_{5/2}$	0.85	108.605	107.16	108.552 (−0.05)		
24–407	$3s^2\ 3p^2(^1_2D)\ ^1D\ 3d\ ^2G_{7/2}$–$3s^2\ 3p^2(^1_2D)\ ^1D\ 4p\ ^2F^o_{5/2}$	0.81	110.732	109.34	110.676 (−0.06)		
19–386	$3s^2\ 3p^2(^1_2D)\ ^1D\ 3d\ ^2F_{7/2}$–$3s^2\ 3p^2(^3_2P)\ ^3P\ 4p\ ^4P^o_{5/2}$	0.65	⋯	107.53	108.963		
23–397	$3s^2\ 3p^2(^3_2P)\ ^3P\ 3d\ ^4D_{7/2}$–$3s^2\ 3p^2(^3_2P)\ ^3P\ 4p\ ^2D^o_{5/2}$	0.63	⋯	107.62	109.024		
39–410	$3s^2\ 3p^2(^3_2P)\ ^3P\ 3d\ ^2F_{7/2}$–$3s^2\ 3p^2(^1_2D)\ ^1D\ 4p\ ^2D^o_{5/2}$	0.59	⋯	119.13	120.962		
15–371	$3s^2\ 3p^2(^3_2P)\ ^3P\ 3d\ ^4F_{5/2}$–$3s^2\ 3p^2(^3_2P)\ ^3P\ 4p\ ^4D^o_{3/2}$	0.54	108.862	107.33	108.802 (−0.06)		
6–392	$3s\ ^2S\ 3p^4(^3_2P)\ ^4P_{5/2}$–$3s^2\ 3p^2(^3_2P)\ ^3P\ 4p\ ^4S^o_{3/2}$	0.33	91.004[D]	89.03	91.013 (0.009)		*
7–392	$3s\ ^2S\ 3p^4(^3_2P)\ ^4P_{3/2}$–$3s^2\ 3p^2(^3_2P)\ ^3P\ 4p\ ^4S^o_{3/2}$	0.28	91.808[D]	89.78	91.817 (0.009)		*
1–593	$3s^2\ 3p^3(^4_3S)\ ^4S^o_{3/2}$–$3s\ ^2S\ 3p^3(^4_3S)\ ^5S\ 4p\ ^4P_{5/2}$	0.28	⋯	62.40	63.24		
1–292	$3s^2\ 3p^3(^4_3S)\ ^4S^o_{3/2}$–$3s^2\ 3p^2(^3_2P)\ ^3P\ 4s\ ^4P_{5/2}$	1.0	79.488	78.29	79.483 (−0.005)		
3–327	$3s^2\ 3p^3(^2_3D)\ ^2D^o_{5/2}$–$3s^2\ 3p^2(^1_2D)\ ^1D\ 4s\ ^2D_{5/2}$	0.83	80.540	79.32	80.545 (0.005)		
1–282	$3s^2\ 3p^3(^4_3S)\ ^4S^o_{3/2}$–$3s^2\ 3p^2(^3_2P)\ ^3P\ 4s\ ^4P_{3/2}$	0.66	80.022	78.78	80.010 (−0.01)		
6–471	$3s\ ^2S\ 3p^4(^3_2P)\ ^4P_{5/2}$–$3s\ ^2S\ 3p^3(^4_3S)\ ^5S\ 4s\ ^4S^o_{3/2}$	0.65	82.672[D]	80.76	82.672 (0.)		*
3–297	$3s^2\ 3p^3(^2_3D)\ ^2D^o_{5/2}$–$3s^2\ 3p^2(^3_2P)\ ^3P\ 4s\ ^2P_{3/2}$	0.60	81.949	80.69	81.950 (0.)		
10–547	$3s\ ^2S\ 3p^4(^1_2D)\ ^2D_{5/2}$–$3s\ ^2S\ 3p^3(^2_3D)\ ^3D\ 4s\ ^2D^o_{5/2}$	0.60	⋯	80.99	82.685		
9–543	$3s\ ^2S\ 3p^4(^1_2D)\ ^2D_{3/2}$–$3s\ ^2S\ 3p^3(^2_3D)\ ^3D\ 4s\ ^2D^o_{3/2}$	0.59	⋯	80.92	82.661		
2–291	$3s^2\ 3p^3(^2_3D)\ ^2D^o_{3/2}$–$3s^2\ 3p^2(^3_2P)\ ^3P\ 4s\ ^2P_{1/2}$	0.58	82.225	81.01	82.247 (0.02)		
6–518	$3s\ ^2S\ 3p^4(^3_2P)\ ^4P_{5/2}$–$3s\ ^2S\ 3p^3(^2_3D)\ ^3D\ 4s\ ^4D^o_{7/2}$	0.47	⋯	78.27	79.603		
5–328	$3s^2\ 3p^3(^2_1P)\ ^2P^o_{3/2}$–$3s^2\ 3p^2(^1_2D)\ ^1D\ 4s\ ^2D_{3/2}$	0.43	82.744	81.47	82.762 (0.018)		
2–328	$3s^2\ 3p^3(^2_3D)\ ^2D^o_{3/2}$–$3s^2\ 3p^2(^1_2D)\ ^1D\ 4s\ ^2D_{3/2}$	0.42	80.160	78.95	80.170 (0.010)		
7–471	$3s\ ^2S\ 3p^4(^3_2P)\ ^4P_{3/2}$–$3s\ ^2S\ 3p^3(^4_3S)\ ^5S\ 4s\ ^4S^o_{3/2}$	0.38	83.336[D]	81.39	83.335 (0.)		*
1–272	$3s^2\ 3p^3(^4_3S)\ ^4S^o_{3/2}$–$3s^2\ 3p^2(^3_2P)\ ^3P\ 4s\ ^4P_{1/2}$	0.34	80.515	79.20	80.499 (−0.016)		*
3–542	$3s^2\ 3p^3(^2_3D)\ ^2D^o_{5/2}$–$3s^2\ 3p^2(^1_2D)\ ^1D\ 4d\ ^2F_{7/2}$	0.97	66.526	65.62	66.529 (0.003)		
3–507	$3s^2\ 3p^3(^2_3D)\ ^2D^o_{5/2}$–$3s^2\ 3p^2(^3_2P)\ ^3P\ 4d\ ^2F_{7/2}$	0.89	67.702 No	66.68	67.551 (−0.15)		?
3–520	$3s^2\ 3p^3(^2_3D)\ ^2D^o_{5/2}$–$3s^2\ 3p^2(^3_2P)\ ^3P\ 4d\ ^4D_{7/2}$	0.83	67.291	66.44	67.293 (0.002)		
2–498	$3s^2\ 3p^3(^2_3D)\ ^2D^o_{3/2}$–$3s^2\ 3p^2(^3_2P)\ ^3P\ 4d\ ^2F_{5/2}$	0.81	67.821 No	66.81	67.706	67.702	N
1–488	$3s^2\ 3p^3(^4_3S)\ ^4S^o_{3/2}$–$3s^2\ 3p^2(^3_2P)\ ^3P\ 4d\ ^4P_{5/2}$	0.75	66.297	65.31	66.324		?
1–493	$3s^2\ 3p^3(^4_3S)\ ^4S^o_{3/2}$–$3s^2\ 3p^2(^3_2P)\ ^3P\ 4d\ ^4F_{5/2}$	0.72	66.047	65.10	66.042 (−0.005)		
5–552	$3s^2\ 3p^3(^2_1P)\ ^2P^o_{3/2}$–$3s^2\ 3p^2(^1_2D)\ ^1D\ 4d\ ^2D_{5/2}$	0.72	67.972 No	66.88	67.822 (−0.15)	67.821	N
3–497	$3s^2\ 3p^3(^2_3D)\ ^2D^o_{5/2}$–$3s^2\ 3p^2(^3_2P)\ ^3P\ 4d\ ^4F_{7/2}$	0.57	⋯	67.11	67.975	67.972	N
1–496	$3s^2\ 3p^3(^4_3S)\ ^4S^o_{3/2}$–$3s^2\ 3p^2(^3_2P)\ ^3P\ 4d\ ^4P_{3/2}$	0.48	65.905	64.97	65.901 (−0.005)		
3–545	$3s^2\ 3p^3(^2_3D)\ ^2D^o_{5/2}$–$3s^2\ 3p^2(^1_2D)\ ^1D\ 4d\ ^2F_{5/2}$	0.46	66.431	65.57	66.486		?
3–561	$3s^2\ 3p^3(^2_3D)\ ^2D^o_{5/2}$–$3s^2\ 3p^2(^1_2D)\ ^1D\ 4d\ ^2G_{7/2}$	0.41	⋯	65.06	65.999		?
4–528	$3s^2\ 3p^3(^2_1P)\ ^2P^o_{1/2}$–$3s^2\ 3p^2(^3_2P)\ ^3P\ 4d\ ^2D_{3/2}$	0.40	68.382	67.43	68.381 (−0.001)		
2–525	$3s^2\ 3p^3(^2_3D)\ ^2D^o_{3/2}$–$3s^2\ 3p^2(^3_2P)\ ^3P\ 4d\ ^2D_{5/2}$	0.38	66.960	66.03	66.972 (0.012)		
5–613	$3s^2\ 3p^3(^2_1P)\ ^2P^o_{3/2}$–$3s^2\ 3p^2(^1_0S)\ ^1S\ 4d\ ^2D_{5/2}$	0.38	⋯	64.41	65.632		?
5–570	$3s^2\ 3p^3(^2_1P)\ ^2P^o_{3/2}$–$3s^2\ 3p^2(^1_2D)\ ^1D\ 4d\ ^2P_{3/2}$	0.34	67.331	66.36	67.321 (−0.02)		
2–548	$3s^2\ 3p^3(^2_3D)\ ^2D^o_{3/2}$–$3s^2\ 3p^2(^1_2D)\ ^1D\ 4d\ ^2D_{3/2}$	0.33	⋯	65.30	66.235	66.224	?
2–545	$3s^2\ 3p^3(^2_3D)\ ^2D^o_{3/2}$–$3s^2\ 3p^2(^1_2D)\ ^1D\ 4d\ ^2F_{5/2}$	0.31	66.232 No	65.38	66.288	66.297	sbl
1–514	$3s^2\ 3p^3(^4_3S)\ ^4S^o_{3/2}$–$3s^2\ 3p^2(^3_2P)\ ^3P\ 4d\ ^4D_{3/2}$	0.27	⋯	64.48	65.386		?
4–612	$3s^2\ 3p^3(^2_1P)\ ^2P^o_{1/2}$–$3s^2\ 3p^2(^1_0S)\ ^1S\ 4d\ ^2D_{3/2}$	0.25	⋯	64.19	65.378		?
1–492	$3s^2\ 3p^3(^4_3S)\ ^4S^o_{3/2}$–$3s^2\ 3p^2(^3_2P)\ ^3P\ 4d\ ^2P_{3/2}$	0.25	⋯	65.16	66.103		?
3–517	$3s^2\ 3p^3(^2_3D)\ ^2D^o_{5/2}$–$3s^2\ 3p^2(^3_2P)\ ^3P\ 4d\ ^4D_{5/2}$	0.22	⋯	66.53	67.382		?
1–501	$3s^2\ 3p^3(^4_3S)\ ^4S^o_{3/2}$–$3s^2\ 3p^2(^3_2P)\ ^3P\ 4d\ ^4P_{1/2}$	0.21	⋯	64.80	65.712		?
1–486	$3s^2\ 3p^3(^4_3S)\ ^4S^o_{3/2}$–$3s^2\ 3p^2(^3_2P)\ ^3P\ 4d\ ^4F_{3/2}$	0.20	⋯	65.39	66.380		?
3–525	$3s^2\ 3p^3(^2_3D)\ ^2D^o_{5/2}$–$3s^2\ 3p^2(^3_2P)\ ^3P\ 4d\ ^2D_{5/2}$	0.20	67.164	66.23	67.175 (0.011)		
1–495	$3s^2\ 3p^3(^4_3S)\ ^4S^o_{3/2}$–$3s^2\ 3p^2(^3_2P)\ ^3P\ 4d\ ^2P_{1/2}$	0.20	⋯	64.98	65.910		?
5–581	$3s^2\ 3p^3(^2_1P)\ ^2P^o_{3/2}$–$3s^2\ 3p^2(^1_2D)\ ^1D\ 4d\ ^2S_{1/2}$	0.15	67.164 No	65.94	66.950		?
3–570	$3s^2\ 3p^3(^2_3D)\ ^2D^o_{5/2}$–$3s^2\ 3p^2(^1_2D)\ ^1D\ 4d\ ^2P_{3/2}$	7.9×10^{-2}	65.805	64.87	65.792 (−0.013)		
2–552	$3s^2\ 3p^3(^2_3D)\ ^2D^o_{3/2}$–$3s^2\ 3p^2(^1_2D)\ ^1D\ 4d\ ^2D_{5/2}$	4.9×10^{-2}	66.221 No	65.17	66.072		?

Note. The relative intensities in Column 3, Int $= N_j A_{ji}/N_e$, are normalized (photons) and are calculated at high density (10^{19} cm^{-3}), using the atomic data in Del Zanna et al. (2012b). Column 4 gives the experimental wavelength λ_{exp} (Å), as in NIST (due to Fawcett) or due to Del Zanna (2012b; [D]). We add a "No" if we consider the previous identification incorrect. Column 5 gives the AUTOSTRUCTURE (AS) wavelength, λ_{AS}. In Column 6, our present wavelength λ_{MCDHF} (with differences with the experimental ones in bracket), while the following column (λ_{rev}) reports the new experimental wavelengths that we propose. The last column indicates if a line is strong in low-density astrophysical plasma (*), if it is blended (sbl), if its identification is questionable (?), or if it is new (N).

Table 4

Transition Wavelengths, λ (in Å); Transition Rates, A (in s^{-1}); Weighted Oscillator Strengths, gf; and Line Strengths, S (in au), between the States of Mn XI (Fe XII, Co XIII, and Ni XIV) Listed in Table 2

Z	i	j	λ	Type	BF	A^l	gf^l	S^l	A^v	gf^v	S^v	Acc.
26	1	2	2.388218E+03	M1	9.992E−01	5.417E+01	1.853E−07	1.094E−01				
26	1	2	2.388218E+03	E2	8.153E−04	4.420E−02	1.512E−10	1.227E−02	4.393E−02	1.502E−10	1.219E−02	B+
26	1	3	2.155836E+03	M1	6.796E−01	2.073E+00	8.667E−09	4.621E−03				
26	1	3	2.155836E+03	E2	3.473E−02	1.060E−01	4.430E−10	2.644E−02	1.055E−01	4.408E−10	2.631E−02	B+
26	1	4	1.341248E+03	M1	7.257E−01	1.889E+02	1.019E−07	3.380E−02				
26	1	4	1.341248E+03	E2	3.788E−04	9.862E−02	5.319E−11	7.644E−04	9.696E−02	5.230E−11	7.515E−04	B+
26	1	5	1.235704E+03	M1	5.511E−01	3.449E+02	3.159E−07	9.652E−02				
26	1	6	3.641427E+02	E1	9.769E−01	1.593E+09	1.900E−01	2.278E−01	1.644E+09	1.961E−01	2.351E−01	B+
26	1	7	3.518149E+02	E1	9.914E−01	1.747E+09	1.297E−01	1.502E−01	1.790E+09	1.329E−01	1.539E−01	A
26	1	8	3.465609E+02	E1	9.910E−01	1.845E+09	6.645E−02	7.581E−02	1.885E+09	6.787E−02	7.744E−02	A
26	1	9	2.939938E+02	E1	1.337E−03	4.892E+06	2.536E−04	2.454E−04	4.905E+06	2.543E−04	2.461E−04	B+
26	1	10	2.923208E+02	E1	2.489E−03	8.219E+06	6.318E−04	6.080E−04	8.329E+06	6.402E−04	6.161E−04	B+
26	1	11	2.564707E+02	E1	4.754E−03	4.416E+07	1.742E−03	1.471E−03	4.342E+07	1.713E−03	1.446E−03	A
26	1	12	2.533862E+02	E1	4.658E−03	4.823E+07	9.284E−04	7.745E−04	4.970E+07	9.569E−04	7.982E−04	B+
26	1	13	2.434208E+02	E1	9.275E−03	7.791E+07	1.384E−03	1.109E−03	7.846E+07	1.394E−03	1.117E−03	A
26	1	14	2.343153E+02	E1	8.934E−02	1.773E+07	5.839E−04	4.504E−04	1.790E+07	5.895E−04	4.547E−04	B+
26	1	15	2.322629E+02	E1	3.065E−01	3.467E+07	1.682E−03	1.287E−03	3.480E+07	1.689E−03	1.291E−03	A
26	1	17	2.259146E+02	E1	9.249E−01	9.726E+07	4.465E−03	3.321E−03	9.764E+07	4.483E−03	3.334E−03	A
26	1	20	2.235926E+02	E1	1.087E−01	7.350E+07	1.102E−03	8.110E−04	7.404E+07	1.110E−03	8.170E−04	B+
26	1	21	2.230702E+02	E1	4.464E−01	3.079E+08	9.189E−03	6.748E−03	3.100E+08	9.252E−03	6.794E−03	A
26	1	22	2.209654E+02	E1	7.735E−01	3.649E+08	1.603E−02	1.166E−02	3.666E+08	1.610E−02	1.171E−02	A+
26	1	23	2.164983E+02	M2	1.037E−05	5.189E+00	2.917E−10	1.324E+00				
26	1	26	1.991910E+02	E1	1.600E−03	1.060E+08	2.522E−03	1.654E−03	1.078E+08	2.565E−03	1.682E−03	A
26	1	27	1.951865E+02	E1	9.793E−01	8.262E+10	2.831E+00	1.819E+00	8.306E+10	2.846E+00	1.829E+00	A+
26	1	28	1.945316E+02	E1	1.044E−01	6.988E+09	7.930E−02	5.078E−02	7.032E+09	7.979E−02	5.110E−02	A+
26	1	29	1.935670E+02	E1	9.914E−01	8.446E+10	1.898E+00	1.209E+00	8.497E+10	1.909E+00	1.217E+00	A+
26	1	30	1.924406E+02	E1	9.250E−01	8.238E+10	9.147E−01	5.795E−01	8.290E+10	9.205E−01	5.832E−01	A+
26	1	31	1.900050E+02	E1	2.305E−01	4.104E+09	8.884E−02	5.557E−02	4.126E+09	8.933E−02	5.588E−02	A+
26	1	32	1.861927E+02	E1	7.855E−02	2.695E+09	8.403E−02	5.151E−02	2.707E+09	8.441E−02	5.174E−02	A+
26	1	34	1.802542E+02	E1	2.061E−03	9.564E+07	2.795E−03	1.659E−03	9.603E+07	2.807E−03	1.666E−03	A

Note. E1 and E2 transition data in both the length (l) and velocity (v) forms are provided. Type is the type of the multipole, and BF is the branching fraction from the upper level. The last column (Acc.) represents the estimated accuracies of the S values using the terminologies of the NIST ASD. Only transitions with BF $\geqslant 10^{-5}$ are presented. A part of the values for Fe XII are shown here for guidance regarding its form and content.

(This table is available in its entirety in machine-readable form.)

#8/$3s\ ^2S\ 3p^4(^3_2P)\ ^4P_{1/2}$, respectively. Our MCDHF1 wavelengths (83.335 and 83.636 Å) for these two transitions show excellent agreement with the observations. The difference between the MCDHF1 excitation energy (1,484,211 cm^{-1}) and the resulting CHIANTI1 experimental energy (1,483,972 cm^{-1}) for the upper level is only −239 cm^{-1}.

The situation for the experimental energies of the $3s^23p^24d$ levels is more complex and Fawcett's identifications of several states are questionable, although we note that none of the transitions are strong in low-density astrophysical plasma. As pointed out by Del Zanna (2012b), the accuracy of previous theoretical wavelengths did not allow firm identifications for the $3s^23p^24d$ levels. In Table 3, we present suggestions for several revised identifications. The experimental excitation energies due to Fawcett et al. (1972) for the $3s^23p^24d$ levels #498, #507, #552, and #581 have large deviations from our MCDHF1 results, with differences between −2800 and −5200 cm^{-1}.

As an example, we consider the transition $3s^2\ 3p^2(^3_2P)\ ^3P\ 4d\ ^2F_{7/2}$–$3s^2\ 3p^3(^2_3D)\ ^2D^o_{5/2}$ between levels #507 and #3. This transition was assigned by Fawcett et al. (1972) to the 67.702 Å line, i.e., with a wavelength about 0.151 Å greater than our MCDHF1 value (67.551 Å). We have noted that the observed wavelength is very close to the MCDHF1 value (67.706 Å) associated with the $3s^2\ 3p^2(^3_2P)\ ^3P\ 4d\ ^2F_{5/2}$–$3s^2\ 3p^3(^2_3D)\ ^2D^o_{3/2}$ transition between levels #498 and #2. The transition rate for this latter (#498–#2) transition is $1.252 \times 10^{11}\ s^{-1}$, which is about two times larger than the rate ($6.804 \times 10^{10}\ s^{-1}$) of the #507–#3 transition, although the two predicted intensities are very similar. Therefore, we suggest to assign the 67.702 Å line to the transition #498/$3s^2\ 3p^2(^3_2P)\ ^3P\ 4d\ ^2F_{5/2}$–#2/$3s^2\ 3p^3(^2_3D)\ ^2D^o_{3/2}$. As a consequence, the NIST (and CHIANTI1) energy for the upper level #498 should be changed to 1,518, 627 cm^{-1}, which agrees with our MCDHF1 1,518,836 cm^{-1} to within 210 cm^{-1}. Similar discrepancies are noted in Table 3.

3.3. Transition Rates and Lifetimes

Wavelengths, λ_{ij}, and the present MCDHF radiative transition data, which include transition rates, A_{ji}; weighted oscillator strengths, gf_{ji}; line strength, S_{ji}; and branching fractions ($BF_{ji} = A_{ji}/\sum_{k=1}^{j-1} A_{jk}$) for electric-dipole (E1), magnetic dipole (M1), electric quadrupole (E2), and magnetic quadrupole (M2) transitions among all the levels listed in Table 2 are reported in Table 4. E1 and E2 radiative transition data are given in both length (l) and velocity (v) forms. Using the uncertainty estimation approach (Kramida 2013, 2014), for E1 and E2 transitions we provide the estimated uncertainties of line strengths S adopting the NIST ASD (Kramida et al. 2018) terminology ($A^+ \leqslant 2\%$, $A \leqslant 3\%$,

$B^+ \leqslant 7\%$, $B \leqslant 10\%$, $C^+ \leqslant 18\%$, $C \leqslant 25\%$, $D^+ \leqslant 40\%$, $D \leqslant 50\%$, and $E > 50\%$) in the last column of this table. The difference, δS, between line strengths S_l and S_v (in length and velocity forms, respectively) is defined as $\delta S = |S_v - S_l| / \max(S_v, S_l)$. The averaged uncertainties, δS_{av}, for line strengths S for E1 transitions Fe XII in various ranges of S are assessed to 1% for $S \geqslant 10^{-1}$, 1.5% for $10^{-1} > S \geqslant 10^{-2}$, 2.7% for $10^{-2} > S \geqslant 10^{-3}$, 6% for $10^{-3} > S \geqslant 10^{-4}$, 12% for $10^{-4} > S \geqslant 10^{-5}$, and 23% for $10^{-5} > S \geqslant 10^{-6}$. Then, the larger of δS_{av} and δS_{ji} is accepted as the uncertainty of each particular line strength. In Table 4, about 24% of E1 S values in Fe XII have uncertainties of $\leqslant$2% (A+), 27% have uncertainties of $\leqslant$3% (A), 29% have uncertainties of $\leqslant$7% (B+), 2.4% have uncertainties of $\leqslant$10% (B), 12% have uncertainties of $\leqslant$18% (C+), 3.6% have uncertainties of $\leqslant$25% (C), and 0.9% have uncertainties of $\leqslant$40% (D+), while only 0.3% have uncertainties of >40% (D and E).

In the spirit of the uncertainty estimation approach (Kramida 2013, 2014), the estimated uncertainties of line strengths S for E2 transitions in Fe XII are estimated, as well as those for E1 and E2 transitions in Mn XI, Co XIII, and Ni XIV. The estimated uncertainties for all E1 and E2 transitions with BF $\geqslant 10^{-5}$ in Mn XI, Fe XII, Co XIII, and Ni XIV are listed in Table 4.

Our MCDHF radiative lifetimes $\tau^l_{\rm MCDHF}$ (in s) in the length form and $\tau^v_{\rm MCDHF}$ (in s) in the velocity form, for the lowest 546 (623, 701, and 745) states of the $3p^4 3d$, $3s3p^2 3d^2$, $3s3p^3 4p$, $3s3p^4$, $3s^2 3d^3$, $3s^2 3p^2 3d$, $3s^2 3p^2 4d$, $3s^2 3p^2 4s$, $3p^3 3d^2$, $3p^5$, $3s3p3d^3$, $3s3p^3 3d$, $3s3p^3 4s$, $3s^2 3p3d^2$, $3s^2 3p^2 4p$, and $3s^2 3p^3$ configurations in Mn XI (Fe XII, Co XIII, and Ni XIV), which are calculated by considering all possible E1, E2, M1, and M2 transitions, are provided in Table 2. Our MCDHF radiative lifetimes $\tau^l_{\rm MCDHF}$ and $\tau^v_{\rm MCDHF}$ show good agreement. For example, the average deviation between $\tau^l_{\rm MCDHF}$ and $\tau^v_{\rm MCDHF}$ for all 623 levels in Fe XII is 1%.

3.4. Summary

Using the MCDHF method combined with the RCI approach, including the transverse electron interaction in the low-frequency limit and the leading QED effects corrections, calculations have been performed for the lowest 546 (623, 701, and 745) levels of the $3p^4 3d$, $3s3p^2 3d^2$, $3s3p^3 4p$, $3s3p^4$, $3s^2 3d^3$, $3s^2 3p^2 3d$, $3s^2 3p^2 4d$, $3s^2 3p^2 4s$, $3p^3 3d^2$, $3p^5$, $3s3p3d^3$, $3s3p^3 3d$, $3s3p^3 4s$, $3s^2 3p3d^2$, $3s^2 3p^2 4p$, and $3s^2 3p^3$ configurations in Mn XI (Fe XII, Co XIII, and Ni XIV). Excitation energies, radiative transition data, and lifetimes are reported.

Our detailed discussion of the excitation energies of the $n = 4$ levels for Fe XII highlights that the identifications are questionable for a few $n = 4$ states. The comparison between experimental and predicted energies clearly shows that the present calculations reach spectroscopic accuracy for these high-lying states. Based on that, several identifications in the other isoelectronic ions are also uncertain. Our calculated excitation energies, as well as radiative transition data, can be used to reliably identify the remaining Fe XII and Ni XIV levels and especially to identify all the $n = 4$ states along the isoelectronic sequence of P-like ions, where very little experimental data are available. The present MCDHF study should therefore stimulate further experimental investigations for those ions. The resulting accurate and consistent MCDHF data set will be useful for astrophysical modeling, line identification work, and also for benchmarking other calculations.

We acknowledge the support from the National Key Research and Development Program of China under grant No. 2017YFA0403200, the Science Challenge Project of China Academy of Engineering Physics (CAEP) under grant No. TZ2016005, the National Natural Science Foundation of China (grant No. 11703004, No. 11674066, No. 11504421, and No. 11734013), the Natural Science Foundation of Hebei Province, China (A2019201300 and A2017201165), and the Natural Science Foundation of Educational Department of Hebei Province, China (BJ2018058). This work is also supported by the Fonds de la Recherche Scientifique (FNRS) and the Fonds Wetenschappelijk Onderzoek—Vlaanderen (FWO) under EOS Project No. O022818F, and by the Swedish research council under contracts 2015-04842 and 2016-04185. G.D.Z. acknowledges support form STFC (UK) via the consolidated grant to the solar/atomic astrophysics group, DAMTP, University of Cambridge. K.W. expresses his gratitude to the support from the visiting researcher program at the Fudan University.

Software: GRASP2K (Jönsson et al. 2007, 2013) and CHIANTI (Dere et al. 1997, 2019) are used in the present work.

ORCID iDs

K. Wang https://orcid.org/0000-0001-6998-1693
G. Del Zanna https://orcid.org/0000-0002-4125-0204
M. Godefroid https://orcid.org/0000-0003-4192-3875
G. Gaigalas https://orcid.org/0000-0003-0039-1163
J. Yan https://orcid.org/0000-0001-6814-5239

References

Behring, W. E., Cohen, L., & Feldman, U. 1972, ApJ, 175, 493
Chen, Z. B., Guo, X. L., & Wang, K. 2018, JQSRT, 206, 213
Chen, Z. B., Ma, K., Wang, H. J., et al. 2017, ADNDT, 113, 258
Del Zanna, G. 2012a, A&A, 537, A38
Del Zanna, G. 2012b, A&A, 546, A97
Del Zanna, G., & Mason, H. E. 2005, A&A, 433, 731
Del Zanna, G., & Mason, H. E. 2018, LRSP, 15, 5
Del Zanna, G., Storey, P. J., Badnell, N. R., & Mason, H. E. 2012a, A&A, 541, A90
Del Zanna, G., Storey, P. J., Badnell, N. R., & Mason, H. E. 2012b, A&A, 543, A139
Dere, K. P., Del Zanna, G., Young, P. R., Landi, E., & Sutherland, R. S. 2019, ApJS, 241, 22
Dere, K. P., Landi, E., Mason, H. E., Monsignori Fossi, B. C., & Young, P. R. 1997, A&AS, 125, 149
Fawcett, B. C., Kononov, E. Y., Hayes, R. W., & Cowan, R. D. 1972, JPhB, 5, 1255
Froese Fischer, C., Godefroid, M., Brage, T., Jönsson, P., & Gaigalas, G. 2016, JPhB, 49, 182004
Gaigalas, G., Froese Fischer, C., Rynkun, P., & Jönsson, P. 2017, Atoms, 5, 6
Gaigalas, G., Zalandauskas, T., & Fritzsche, S. 2004, CoPhC, 157, 239
Grant, I. P. 2007, Relativistic Quantum Theory of Atoms and Molecules (New York: Springer), doi:10.1007/978-0-387-35069-1
Guo, X. L., Huang, M., Yan, J., et al. 2015, JPhB, 48, 144020
Guo, X. L., Si, R., Li, S., et al. 2016, PhRvA, 93, 012513
Jönsson, P., Gaigalas, G., Bieroń, J., Froese Fischer, C., & Grant, I. P. 2013, CoPhC, 184, 2197
Jönsson, P., Gaigalas, G., Rynkun, P., et al. 2017, Atoms, 5, 16
Jönsson, P., He, X., Froese Fischer, C., & Grant, I. 2007, CoPhC, 177, 597
Kramida, A. 2013, Fusion Sci. Tech., 63, 313
Kramida, A. 2014, ApJS, 212, 11
Kramida, A., Ralchenko, Yu., Reader, J. & NIST ASD Team 2018, NIST Atomic Spectra Database v5.6.1 (Gaithersburg, MD: STScI)
Si, R., Li, S., Guo, X. L., et al. 2016, ApJS, 227, 16
Si, R., Zhang, C., Liu, Y., et al. 2017, JQSRT, 189, 249
Si, R., Zhang, C. Y., Cheng, Z. Y., et al. 2018, ApJS, 239, 3

Storey, P. J., Del Zanna, G., Mason, H. E., & Zeippen, C. J. 2005, A&A, 433, 717
Tayal, S. S. 2011, ADNDT, 97, 481
Vilkas, M. J., & Ishikawa, Y. 2004, JPhB, 37, 4763
Wang, K., Chen, Z. B., Si, R., et al. 2016a, ApJS, 226, 14
Wang, K., Chen, Z. B., Zhang, C. Y., et al. 2018a, ApJS, 234, 40
Wang, K., Guo, X. L., Liu, H. T., et al. 2015, ApJS, 218, 16
Wang, K., Jönsson, P., Del Zanna, G., et al. 2020, ApJS, 246, 1
Wang, K., Jönsson, P., Ekman, J., et al. 2017a, PhRvL, 119, 189301
Wang, K., Jönsson, P., Ekman, J., et al. 2017b, JQSRT, 194, 108
Wang, K., Jönsson, P., Ekman, J., et al. 2017c, ApJS, 229, 37
Wang, K., Jönsson, P., Gaigalas, G., et al. 2018b, ApJS, 235, 27
Wang, K., Li, D. F., Liu, H. T., et al. 2014, ApJS, 215, 26
Wang, K., Li, S., Jönsson, P., et al. 2017d, JQSRT, 187, 375
Wang, K., Si, R., Dang, W., et al. 2016b, ApJS, 223, 3
Wang, K., Song, C. X., Jönsson, P., et al. 2018c, ApJS, 239, 30
Wang, K., Zhang, C., Jönsson, P., et al. 2018d, JQSRT, 208, 134
Wang, K., Zheng, W., Zhao, X. H., et al. 2019, JQSRT, 236, 106586
Young, P. R., Watanabe, T., Hara, H., & Mariska, J. T. 2009, A&A, 495, 587
Zhao, Z., Wang, K., Li, S., et al. 2018, ADNDT, 119, 314